J. Physiol. (1976), **254**, *pp.* 245–283
With 18 *text-figures*
Printed in Great Britain

A NON-LINEAR VOLTAGE DEPENDENT CHARGE MOVEMENT IN FROG SKELETAL MUSCLE

BY W. K. CHANDLER, R. F. RAKOWSKI* AND M. F. SCHNEIDER†

From the Department of Physiology, Yale University School of Medicine, 333 Cedar Street, New Haven, Connecticut, U.S.A.

(*Received 13 February 1975*)

SUMMARY

1. Voltage-clamp experiments were carried out using the three microelectrode technique. Using this method membrane current density at V_1 is proportional to $\Delta V(=V_2-V_1)$ where V_1 and V_2 are voltages at distances l and $2l$ from the end of a fibre. Voltage dependent sodium currents were blocked by tetrodotoxin, potassium currents by tetraethylammonium ions and rubidium. Contraction was blocked by adding sucrose, 467 mM.

2. The current ΔV(control) associated with a positive voltage step from a hyperpolarized conditioning voltage to the holding potential, -80 mV, showed two components, a capacitative transient which decayed rapidly and a maintained steady level. The current ΔV(test) associated with the same size positive step from the holding potential showed the same two components plus a third one, a transient current which usually decayed more slowly than the capacitative transient. The third component is best seen by subtracting the first two components, obtained from ΔV(control), from ΔV(test), to give ΔV(test-control).

3. The difference trace ΔV(test-control) showed a transient outward current during pulse 'on', as mentioned above, and a transient inward current during pulse 'off'. The rates of decay of the 'on' and 'off' transients were, in general, different. The 'on' rate depended on the voltage during the pulse, the 'off' rate did not.

4. The total charge which moved during the 'on' transient, evaluated as the time integral of current, was equal in magnitude but opposite in direction to that which moved during the 'off'.

5. The amount of charge movement Q bears a sigmoid relationship to voltage. A simple equation which describes this behaviour is

$$Q = \frac{Q_{\max}}{1+\exp[-(V-\bar{V})/k]}.$$

* Present address: Department of Physiology and Biophysics, Washington University School of Medicine, St Louis, Missouri, U.S.A.

† Present address: Department of Physiology, University of Rochester School of Medicine, Rochester, New York, U.S.A.

Data from six fibres gave average values $Q_{max} = 25$ nC/μF (normalized by fibre capacitance), $\bar{V} = -44$ mV, $k = 8$ mV.

6. The simplest interpretation of these results is to suppose that there are a fixed number of charged groups confined to the membrane but free to move reversibly between at least two different sites which see different proportions of the total membrane potential.

7. The average values for Q_{max} and k give a density of charged groups of $5{\cdot}1 \times 10^{10}$ groups/μF. Using 0·9 μF/cm^2 for capacitance/area there are 459 groups/μm^2 averaged over surface and tubular membranes. If the groups are located only in the tubules the density would be 500–600/μm^2.

8. An analysis of the passive electrical properties in terms of the Falk & Fatt (1964) model gave values for the tubular time constant which ranged from 1·50 to 3·04 msec. Theoretical reconstructions of charge movement currents were carried out assuming that the groups are distributed uniformly according to surface and tubular capacitance. The results indicate that tubular delays would distort the current transients if much of the charge is located in the T-system.

9. A theoretical analysis was carried out using two simple circuits consisting of a constant capacitance, due to either T-system or sarcoplasmic reticulum (S-R), in series with a voltage dependent conductance. The results indicate that changes in the voltage dependent conductance, either instantaneous or time dependent, cannot account for the observed charge movement currents.

INTRODUCTION

When a frog skeletal muscle fibre is depolarized for a few tenths of a second, contraction is activated if the membrane potential is made more positive than a threshold value, somewhere near -50 mV (Hodgkin & Horowicz, 1960; Adrian, Chandler & Hodgkin, 1969). The activation is controlled by the voltage across the membranes of the transverse tubular or T-system (Huxley & Taylor, 1958; Huxley & Straub, 1958) and it is this voltage which somehow plays a major role in regulating calcium release from the sarcoplasmic reticulum (Ebashi, Endo & Ohtsuki, 1969). Since activation is strongly voltage dependent it is natural to wonder whether a step in the activation mechanism involves physical movement of a charged molecule or part of a molecule in response to the change in electric field produced within the membrane by depolarization. If such a process were involved in activation, the movement or re-orientation of charge would contribute to the membrane current, and under favourable circumstances this component might possibly be detected.

With these ideas in mind Schneider & Chandler (1973) carried out voltage-clamp experiments on frog sartorius fibres, using the three micro-

electrode technique, to look for a current fitting the above description. The strategy of the experiments was (1) to eliminate voltage and time dependent sodium and potassium currents with tetrodotoxin and tetraethylammonium ions (TEA), (2) to suppress mechanical movement with sucrose hypertonicity, a step which was necessary to allow use of the micro-electrode method, and (3) to subtract the usual capacitative component from the records by taking the difference between a test voltage step into the region where activation occurs (which would give capacitative current plus any 'activating' current) and a control step of equal magnitude superimposed on a conditioning hyperpolarization (which would give only the capacitative component).

Under these conditions the difference in currents associated with the test and the control pulses consistently showed a transient outward component on depolarization followed by a transient inward component on repolarization. The total amount of extra charge which moved during the 'on' transient, obtained as the time integral of the current, was equal to that observed when the pulse was switched off. This equality held when the amount of charge which moved was varied, either by changing the level or the duration of the pulse. These findings suggest that the charges which move one way on depolarization move back when the fibre is repolarized. Furthermore, the relationship between charge movement and potential saturates, indicating that there is a maximum amount of charge which is movable.

The simplest interpretation of these results is to suppose that there are a fixed number of charged groups confined to the membrane but free to move reversibly between at least two different sites which see different proportions of the total membrane potential. The aim of this paper is to provide a more detailed description of the charge movement currents and of the experimental method used for their measurement. Some of the results have been described already (Chandler, Schneider, Rakowski & Adrian, 1975).

METHODS

A diagram of the apparatus used for voltage clamp is shown in Fig. 1. The method is similar to that used by Adrian, Chandler & Hodgkin (1970*a*). Three micro-electrodes were inserted into a fibre near the pelvic end of the sartorius muscle of *Rana temporaria*. Two of the electrodes, filled with 3 M potassium chloride, were inserted at distances $x = l$ and $x = 2l$ from the end; these were used to measure potentials V_1 and V_2 respectively. A third electrode, filled with 2 M potassium citrate, was used to pass current, I. Electrode resistances ranged from 5 to 10 MΩ. Voltage recording electrodes had tip potentials of less than 5 mV. According to the steady-state theory developed by Adrian *et al.* (1970*a*) i_m, the current density at $x = l$, is closely approximated by

$$i_m = \frac{2(V_2 - V_1)}{3l^2 r_i}, \qquad (1)$$

where r_1 is the internal longitudinal resistance per unit length. A similar theoretical approach (Schneider & Chandler, 1976) indicates that the time integral of eqn. (1) can be used to give the amount of charge placed across the fibre capacitance during a voltage step. It is this application of eqn. (1) which is important for the charge movement experiments.

The V_1 and V_2 electrodes were surrounded with aluminium foil shields driven by the outputs of the respective unity gain electrometers. With the electrode tip barely touching the solution, a voltage step on the bath produced an almost exponential

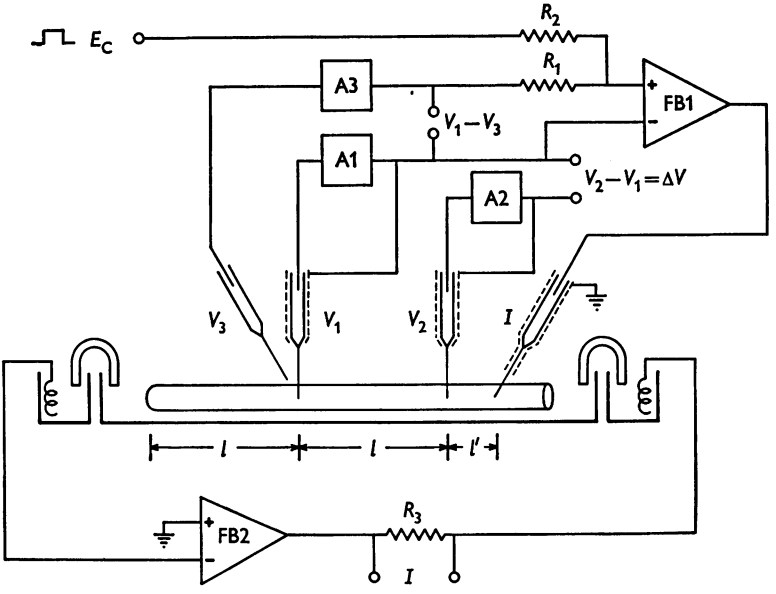

Fig. 1. Diagram of experimental apparatus. A1, A2 and A3 represent unity gain FET input electrometer followers. Two internal micro-electrodes (V_1 and V_2) were inserted into a muscle fibre so that V_1 was equidistant from the end of the fibre and from V_2. A third internal micro-electrode was used to pass current. The transmembrane potential at V_1 was measured as the difference between the potential recorded by the internal micro-electrode and an external reference electrode (V_3). The recorded membrane potential was compared with a command signal (E_c) and was used in a feed-back configuration to drive the current passing electrode. The command potential steps were not perfectly square but were intentionally rounded with an exponential time constant of 40 μsec. FB1 represents a vertical amplifier in a Tektronix 502A oscilloscope (gain 500–2000) followed by an operational amplifier (model 170, Analog Devices) used as an inverter with a gain of 7. To prevent its going into saturation the 170 amplifier's input signal was diode limited so that its output voltage remained within $\pm$ 95 V. The total electrode current to earth, I, was measured as the potential drop across resistor R_3 which is in the feed-back loop of an operational amplifier (FB2) (model 149B, Analog Devices). FB2 maintains the bath at earth potential. The membrane current density at V_1 is proportional to ΔV, $(= V_2 - V_1)$, according to eqn. (1). See text for further details. R_1 = 10 kΩ, R_2 = 200 kΩ, R_3 = 50 kΩ.

response with a time constant of 5–8 μsec for 5–7 MΩ electrodes. The screen for the current passing electrode was at earth potential.

The amplifier FB2 clamped the periphery of the bath at earth potential. During the make and break of a voltage step, when the total current was large but transient, external potentials of 5–30 mV with respect to earth could develop in the vicinity of the V_1 or V_2 electrodes. This signal was measured by an external micro-electrode V_3 and 0·95 ($= R_2/[R_1+R_2]$) of the signal was applied to the feed-back amplifier FB1 so that $V_1 - 0{\cdot}95\,V_3$ was the controlled voltage.

$V_1 - V_3$ and $\Delta V (= V_2 - V_1)$ were displayed on a Tektronix 565 oscilloscope and photographed. In addition, slow changes were followed on a Brush Model 280 two channel chart recorder.

The solution used contained 117·5 mM tetraethylammonium Cl (TEA Cl), 5 mM-RbCl, 1·8 mM-$CaCl_2$ and tetrodotoxin 10^{-6} g/ml.; 467 mM sucrose was added to prevent mechanical movement. pH was maintained at 7·1 with 1 mM Tris maleate buffer. The chamber was mounted on a thermoelectric device (Cambion) which was used to lower the bath temperature to 0–2° C, measured by a small thermistor placed near the muscle. The chamber, microscope and micromanipulators were placed on a vibration isolation table (Lansing isolation system 71.402 plus top 72.504) to minimize the effects of mechanical vibrations in the room.

Digital processing of data

The signals V_1–V_3 (which will be written hereafter simply as V_1), ΔV and I were also recorded by a PDP-8/e computer system on-line for subsequent analysis. The special interfacing, described below, was designed and constructed in the Instrumentation Laboratory in the Department of Physiology, Yale University School of Medicine. Each of the electrical signals was amplified by an instrumentation amplifier (Analog Devices AD520J) with an adjustable gain of 25, 50, 100 or 200. The output was followed by a high frequency operational amplifier filter of conventional design. The high frequency cut-off was set at 1 kHz for V_1 and ΔV and at 0·1 kHz for I.

The amplified and filtered signal was then applied to a voltage-to-frequency (V-F) converter (Anadex 1700-5044-00), the output frequency of which varied linearly with input voltage, 0·1 MHz/V, over the range 0–12 V. The input voltage was limited by a diode network to prevent overload. The V-F output pulses were counted during successive 1 msec intervals. Since the number of counts during a precisely timed interval is directly proportional to the average value of input voltage during the interval, this method provides a means for converting an analogue signal into digital form. The method is particularly useful if the time integral of the input signal is required, as was the case for the experiments reported here. A disadvantage is that temporal resolution is somewhat sacrificed. In order to measure either positiveor negative signals, a DC bias of 8 V was used and the input voltage was restricted to ± 4 V.

The voltage-clamp command pulses as well as the timing marks for the counters following each V-F converter were produced by two digital stimulator units, timed by the same crystal clock. These units were also designed and built in the Instrumentation Laboratory of the Department. Fig. 2 is a diagram of the pattern of pulses used. Trace *A* shows the initial and final segments of a command pulse. In the experiments the rising and falling phases of the pulse were lagged by a 40 μsec time constant to decrease ringing. Trace *B* shows two portions of a train of timing pulses, 10 μsec duration, frequency 1 kHz. The train started exactly 50 msec before the pulse in trace *A* so that if 0 is used for the first mark number, the leading edge of mark number 50 coincides with the beginning of the step. Number 150 coincides with the end of the step in this example.

When the counter for a V-F converter receives a timing mark, the following sequence of events occurs: (1) the input to the counter is disabled, (2) the number in the counter is transferred to a storage buffer, (3) a 'flag' is set which the computer can sense, (4) the counter is zeroed and (5) the input to the counter is enabled. These steps are carried out in about 4 μsec. During the next 996 μsec, while the next interval is being counted, the computer transfers the number in the storage buffer to core memory and clears the 'flag'. In this way a total of 256 sequential points are sampled during a sweep. Trace C in Fig. 2 is a diagram of the counts from the V-F converter using trace A as the input. Each point is proportional to the average value of record A for the preceding 1 msec interval. Points 51 and 151 are about 4% from the final levels owing to the 40 μsec rounding on trace A.

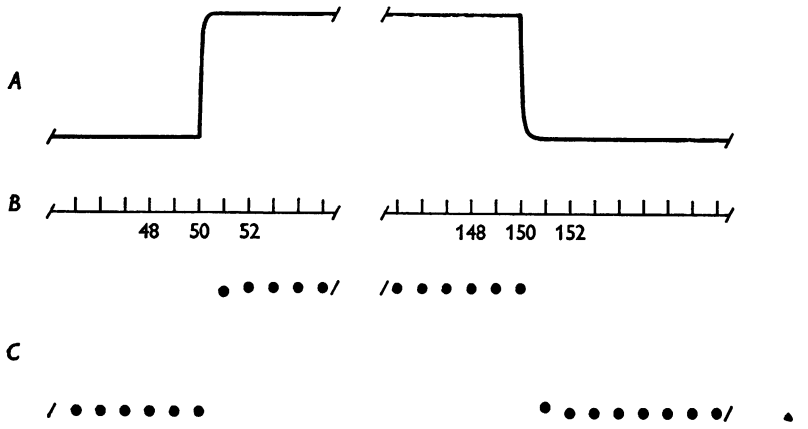

Fig. 2. Diagrammatic representation of a pulse sequence used for the experiment. Trace A shows the command voltage step. The rising and falling phases of the command step are exponentially rounded with a time constant of 40 μsec. The rounding has been accentuated in the Figure. Trace B indicates timing marks, repeated at 1 msec intervals, used to trigger the counters following the V-F converters. The timing marks are synchronized with the 'on' and 'off' of the command pulse. Trace C represents the output of a counter following a V-F converter with trace A as input. See text for additional information.

In the experiments a separate V-F converter and counter combination was used for each of the signals V_1, ΔV and I. All counters were triggered simultaneously by the same timing pulse train. ΔV was also recorded simultaneously with a conventional sample and hold amplifier (Analogic Model MP270) and high speed 12 bit A/D converter (Analogic Model MP 2912A).

At the end of each sweep the data points were transferred to an RK8E disk for storage during the experiment. At the end of an experiment the data were transferred from the disk to magnetic (DEC) tape for long term storage.

The computer programmes used for data acquisition and preliminary analysis during the experiment were written in PAL-8 assembly language. Subsequent analysis was performed using programmes written in a higher level language, usually OS-8 FORTRAN IV and occasionally BASIC. Permanent records were plotted on a digital incremental plotter (Calcomp Model 565).

Analysis of cable parameters

At the beginning of each experiment cable properties were measured in a manner similar to that described by Adrian *et al.* (1970*a*). The voltage electrode used for feed-back control was changed for these measurements from V_1 to V_2 and steps of ± 10 mV lasting 100 msec were applied. The high frequency cut-off for ΔV and V_2 was changed from 1 to 20 kHz. Values of λ and r_i were calculated from the relations

$$\lambda = \sqrt{\frac{3l^2 V_1}{2\Delta V}}, \tag{2}$$

$$r_i = \frac{V_1 \cosh[(2l+l')/\lambda](1+\tanh[(2l+l')/\lambda])}{I\lambda \cosh(l/\lambda)}, \tag{3}$$

which follow from eqns. (9) and (11) of Adrian *et al.* (1970*a*), using steady-state values for V_1 (taken relative to the holding potential), ΔV and I. λ is the space constant of the fibre; l and l' are the spacing of the electrodes as shown in Fig. 1. From the definition of space constant,

$$\lambda = \sqrt{\frac{r_m}{r_i}}, \tag{4}$$

it is possible to calculate r_m, the fibre membrane resistance times unit length, once λ and r_i are determined.

Values of $r_i c_m$, where c_m is the fibre capacitance per unit length, were obtained from analysing the areas under the V_1 and ΔV curves during the 'on' and 'off' portions of the step. This method is described in detail in a subsequent paper (Schneider & Chandler, 1976).

RESULTS

Voltage V_1 during a step

Fig. 3 shows records of V_1(line *a*) and ΔV(line *b*) for control (column *A*) and test (column *B*) conditions. Each point in the records gives the average value of voltage taken over a 1 msec interval, according to the procedure outlined in the Methods section.

Fig. 3*Aa* shows the time course of V_1 when a 50 mV depolarizing pulse was superimposed on a longer duration 50 mV hyperpolarizing conditioning pulse. Since the depolarizing and hyperpolarizing pulses had equal amplitudes the potential during the positive pulse was equal to the holding potential; this strategy was usually used for control measurements. The first fifty points show the base-line voltage before the depolarizing pulse. The next point (number 51) gives the average voltage during the first msec of the step, $-91{\cdot}5$ mV. This corresponds to a change in voltage of 38·5 mV from the conditioning level or 0·77 times the final 50 mV step size. Since the pulses which determine the sampling intervals are synchronized exactly with the command pulse the failure to register the full 50 mV cannot be attributed to the sampling interval beginning prior to the voltage step. Rather the factor 0·77 represents delays associated with the measured value of V_1 reaching its steady level. The total delay, which is

comparable to a single time constant of 0·23 msec, is due to several factors: (1) the 0·04 msec delay imposed on the command pulse, (2) the delay in the command potential being realized at $x = l$ and (3) the 0·16 msec delay introduced by the filter network in the recording amplifier. If all the delays were exponential the individual time constants should add to give

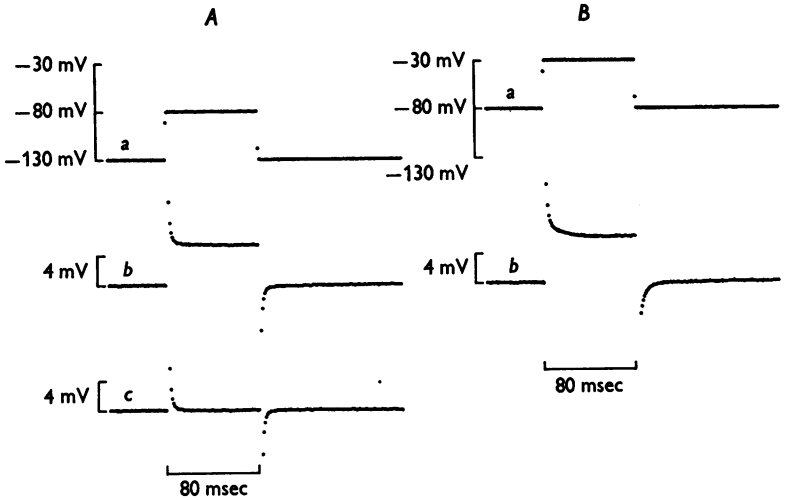

Fig. 3. Records of V_1 and ΔV for a control (A) and test (B) voltage step. Each trace is the average of four records; each point represents the average value during a 1 msec interval. *Aa* shows the control potential step recorded at V_1. A hyperpolarizing prepulse to $V_1 = -130$ mV, duration 390 msec, was initiated 100 msec before the depolarizing step. *Ab* shows the ΔV record. *Ac*, which represents only the capacitative current, was obtained from *Ab* by subtracting sloping base lines as described in the text. *Ba*, *Bb* are records associated with the test pulse. They are similar to *Aa*, *Ab* except that no prepulse was used. In the ΔV records (*Ab*, *Ac* and *Bb*) the first three points of the 'make' and 'break' of the step have been omitted. Trace *Ac* is shown again in Fig. 7*Ad* at lower gain. Electrode spacing $l = 191$ μm, $l' = 19$ μm. Cable measurements gave $\lambda = 0{\cdot}0831$ cm, $r_i = 10{\cdot}62$ MΩ/cm, $c_m = 0{\cdot}2303$ μF/cm; therefore 1 mV on ΔV corresponds to 0·172 μA/cm (eqn. (1)) or 0·751 μA/μF. Fibre 10.2, 1·4° C. Initial resting potential, −67 mV; holding potential, −80 mV.

the total, 0·23 msec. Delays (1) and (3) are both exponential and therefore account for 0·20 msec, leaving an effective delay of 0·03 msec associated with V_1 following the command pulse.

Data points 52–130 show the steady level of V_1 during the pulse and points 131–255 show V_1 when the command pulse was turned off.

In Fig. 3*Ba* the same magnitude depolarizing pulse was applied from the holding potential; this constituted the test condition to be compared with the control pulse configuration illustrated in Fig. 3*Aa*.

Control and test ΔV traces

Fig. 3*Ab* shows the time course of the ΔV(control) record corresponding to the V_1 record in Fig. 3*Aa*. On depolarization there was a large outward current associated with capacitative charging of the membranes. This rapidly decayed to an almost steady level of ionic current. At this gain it was necessary to omit the first three data points at the 'on' and 'off' of the step in the ΔV traces.

In order to separate capacitative from ionic current components, the data points from number 55 (the fifth point after the step) to number 130 (the last point of the step) were fitted by a sloping base line plus an exponential term

$$\Delta V = c_1 + c_2 t + c_3 \exp(-t/\tau). \quad (5)$$

The use of this equation is based on the assumption that the slight variation in ionic current during the pulse was linear with time. The exponential term was introduced only as a curve fitting convenience to allow for the final decay of the capacitative component; it was not used further in the analysis. The fitting procedure for this and subsequent analyses was to adjust c_1, c_2, c_3 and τ to give a minimum value of the squared deviations. The calculations were done with a computer programme that operated in an interactive mode and that displayed both the data and the calculated best fit. In this record a value of 2·44 msec for τ gave a best fit. The same procedure applied to the 'off' response gave a similar value for τ, 2·21 msec.

The trace in Fig. 3*Ac* shows ΔV with the ionic components removed. The linear components ($c_1 + c_2 t$ in eqn. 5) were subtracted from the 'on' and 'off' segments, and the initial base line was also corrected for slope. The latter correction was necessary since small, slow changes in inward current occurred for large hyperpolarizations. This may reflect properties either of ingoing rectifier currents which had not been blocked by TEA and rubidium outside (Adrian & Freygang, 1962; Adrian, Chandler & Hodgkin, 1970*b*) or of the chloride currents (Warner, 1972). The trace in Fig. 3*Ac*, then, gives the currents associated with capacitative charging alone.

Fig. 3 *Bb* shows ΔV(test) when the step was applied from the holding potential, −80 mV. The 'on' transient shows two components, a rapidly decaying current plus a more slowly decaying one. The rapid component resembles the transient seen in record *Ab*, suggesting that it represents the usual linear capacitative current. On the other hand, the more slowly decaying current in *Bb* is not present in *Ab*.

The 'off' responses in Fig. 3*Ab* and *Bb* are also not identical, although the difference is less obvious. In *Bb* the current is larger than *Ab* and the return to the base line is slower.

Difference traces, test minus control

The difference between traces *Bb* and *Ab* in Fig. 3 is best seen by subtraction. Firstly, though, it is important to check that the actual magnitudes of the voltage step V_1 in Fig. 3*Aa* and *Ba* are the same. This ensures that the currents associated with changing the voltage across the linear components of capacitance subtract exactly. In the experiment in Fig. 3 the average voltage in *Ba* was 1·0007 times that in *Aa*, showing that the voltage steps were essentially equal. In subsequent stages of analysis the control records for V_1 and ΔV were multiplied by this correction factor. Correction factors were routinely calculated in all experiments and were usually within 1 % of unity.

Fig. 4*A* shows V_1(test) and 4*B* shows V_1(test) minus V_1(control). The

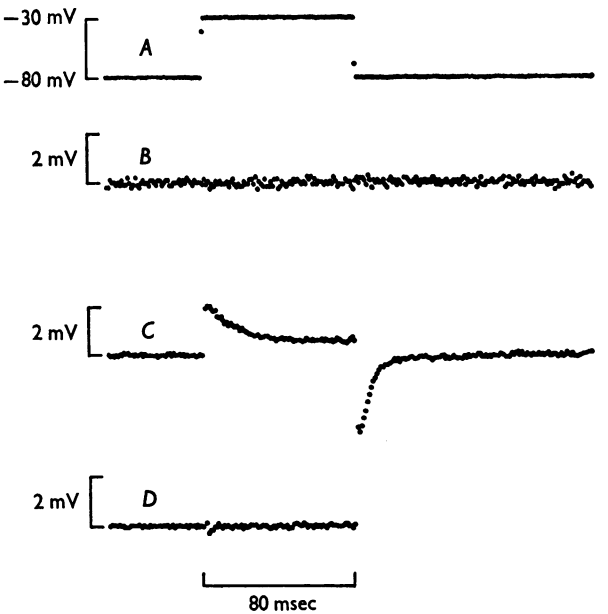

Fig. 4. Difference traces, test minus control. Trace *A* shows voltage V_1 during the test voltage step, same as Fig. 3*Ba*. Trace *B* shows V_1(test) minus V_1(control), i.e. trace 3*Ba* minus 3*Aa*. Trace *C* shows the difference in ΔV traces, 3*Bb* minus 3*Ac* minus a constant current during the pulse given by resting conductance times voltage displacement. Records of this type are referred to as ΔV(test-control). Trace *D* was obtained by adding the first 80 msec of the 'on' and the 'off' currents in 3*Ac*. This record shows that the control capacity charging currents were symmetrical. The subtracted voltage record, trace *B*, is noisier than *C* and *D* because the gain of the V_1 amplifier was one fourth the gain of the ΔV amplifier. Same experiment as Fig. 3.

difference is uniformly zero indicating that the time courses of the test and control voltage steps at V_1 were identical.

The difference ΔV trace, ΔV(test-control), is shown in Fig. 4*C*. This was obtained in two stages. Firstly, record *Ac* in Fig. 3 was subtracted from *Bb*. Any capacitative current due to linear capacitative elements should be identical in both records and thus cancel out. Next, most of the ionic current accompanying the test step was eliminated by subtracting resting conductance times voltage displacement. The result, Fig 4*C*, shows a transient outward current during the pulse followed by a transient inward current on repolarization. It is apparent that the inward current decayed more rapidly than the outward current, making the record asymmetrical. On the other hand, the control capacitative charging transients for pulse 'on' and 'off' were symmetrical (Fig. 4*D*).

The small, steady level of current at the end of the depolarizing pulse in Fig. 4*C* reflects a slight non-linearity in the ionic I–V curve for the fibre. This would be expected if movements of chloride or potassium ions, for example, followed a constant field type rectification.

Non-linear capacitative current or charge movement

The record in Fig. 4*C* is shown again in Fig. 5*A* with straight lines representing the ionic currents drawn as described in the legend. Subtraction of the ionic components gives Fig. 5*B*. This record shows the extra transient component of current associated with a 50 mV pulse from −80 mV, a component not present when the pulse was applied from −130 mV.

Some of the properties of this current have been described by Schneider & Chandler (1973) who concluded that it represents the motion of charges or dipoles, confined to the membrane phase, but free to move between different locations or angular orientations within the membrane. A strong argument in favour of this explanation is that the amount of charge, equal to the time integral of the current, which moves one way during the pulse 'on' is equal to that which moves back during the 'off'. Fig. 5*C* shows the cumulative area or time integral of Fig. 5*B*. The values have been normalized for total fibre capacitance. Although the units after normalization are most simply given as mV, we have used nC/μF to emphasize that the units represent charge divided by capacitance. Since the capacitance of surface and T-system membrane is about 0·9 μF/cm^2 (Schneider, 1970; Hodgkin & Nakajima, 1972) the value in units nC/μF roughly corresponds to nC/cm^2.

In Fig. 5*C* the total charge which moved during the pulse 'on' reached a steady level of 17·5–18·0 nC/μF, with an average value of 17·8 nC/μF. After the pulse the area returned slightly below zero, about −0·6 nC/μF.

Since the currents associated with the charge movement are small it was important for the measurements that relatively high gains in the instrumentation amplifiers be used. This meant that the ΔV trace at the beginning and end of the pulse went out of range during the first part of the first msec, thereby resulting in an error in the first point. It is not obvious how to assign a value for the point and we arbitrarily set the value of the first point equal to the value of the second. In Fig. 4*C* the first

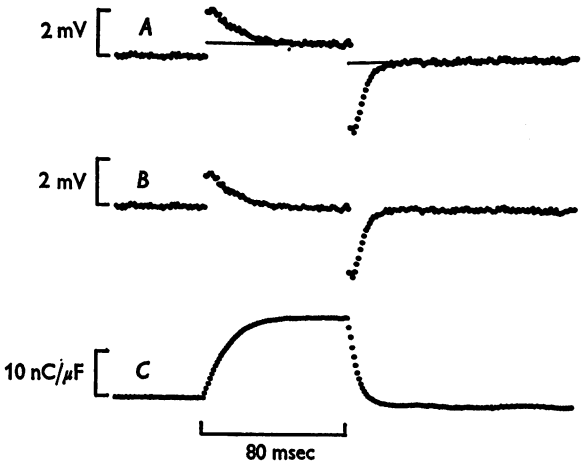

Fig. 5. Determination of charge movement. Trace *A* gives ΔV(test-control) from Fig. 4*C* with lines showing the ionic currents. The line during the pulse is given by $c_1 + c_2 t$ in eqn. (5) which was fitted from points 70 to 130. The line after the pulse was fitted from points 140 to 255. Trace *B*, which was obtained by subtracting the ionic currents in *A*, shows the transient, non-linear capacitative current or charge movement. Trace *C* is the time integral of *B* beginning with the first point during the pulse. The units in *C* have been scaled by fibre capacitance. Same experiment as Fig. 3.

points after the 'on' and 'off' are not shown; in Fig. 5*A* and *B* the first points have been set equal to the second. In terms of area the effects of this procedure are rather small; in Fig. 5*C* the first 'on' value (set equal to the second value) corresponds to about 6 % of the total charge and the first 'off' value to about 12 %.

Charge movement currents at different potentials

Fig. 6*A* shows ΔV(test-control) records for different test potentials as indicated at the left. The procedure was similar to that shown in Fig. 3. The 'test' pulses were superimposed on the holding potential whereas the 'control' pulses were superimposed on hyperpolarizing conditioning prepulses. The potential of the prepulse was chosen so that the voltage during

the positive pulse was equal to the holding potential. This procedure permitted the subtraction of a control record in which the direction of microelectrode current was the same as in the test record.

Control records for the first five traces in Fig. 6*A* are shown in Fig. 7*A*. For the sixth record in Fig. 6*A*, V_1 = 18 mV, the control record was the sum of two half size pulses similar to Fig. 7*Ad*; for V_1 = 67 mV the sum of three pulses, each one third size, was used. Fig. 7*B* shows that the control

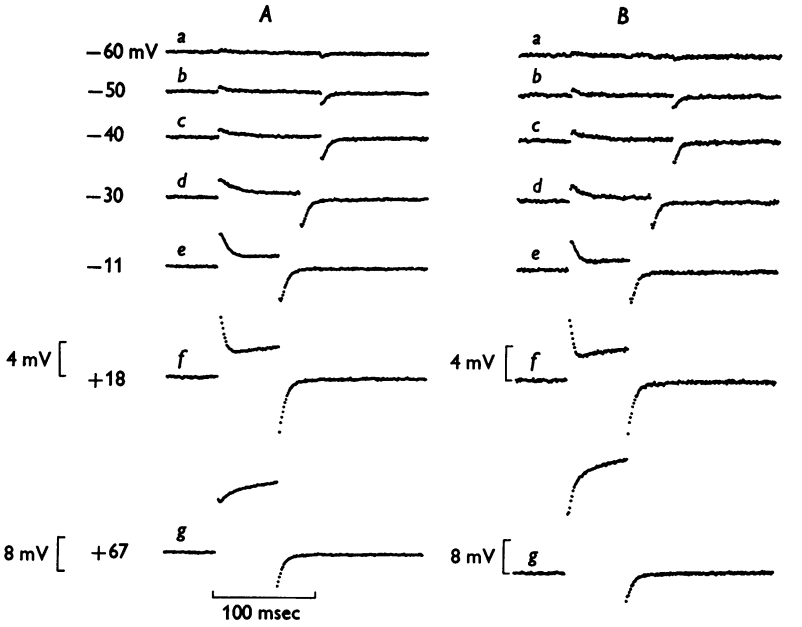

Fig. 6. ΔV(test-control) for different voltages. *A*, average of four runs with test voltages indicated at left. A control pulse followed by a test pulse was done for −60 mV, then for −50 mV, and progressively more positive to +67 mV. This sequence was then repeated a total of four times. *B*, first run of the sequence. Note lower gain of the bottom records. The correction factors (= V_1(test)/V_1(control)) ranged from 0·9964 to 1·0012. Fibre 10.2, same experiment as Fig. 3.

records all scale linearly according to the magnitude of the voltage step. In addition, for each control record the 'on' and 'off' transients were symmetrical; i.e. the sum of the two gave a flat trace similar to Fig. 4*D*. This behaviour indicates that within the voltage range −80 to −150 mV the capacitative properties are approximately linear so that the particular method used for determining the control record is not critical.

Inspection of the records in Fig. 6*A* shows that as the internal potential was made more positive than −40 mV the peak value of transient current

due to charge movement increased as did its rate of decay. At 18 mV there was a gradual increase in current throughout the pulse, after the charge movement transient. Since the control traces have had ionic currents subtracted, this increase occurred during the test pulse, possibly due to the slow conductance change described by Adrian *et al.* (1970*b*). These changes in current are more pronounced in the record at 67 mV.

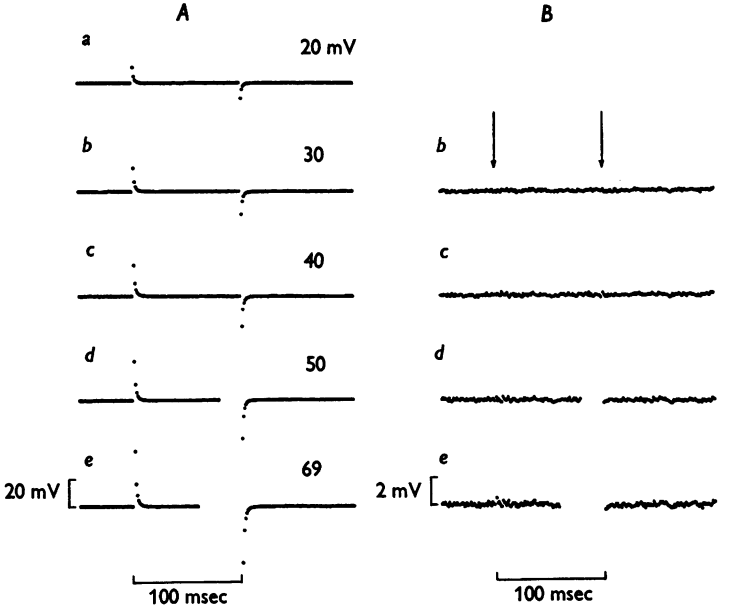

Fig. 7. Linearity of control ΔV transients for different magnitude pulses. *A*, currents associated with pulses to −80 mV from conditioning prepulse voltages −100 mV (trace *a*), −110 mV (*b*), −120 mV (*c*), −130 mV (*d*) and −149 mV (*e*). The magnitude of the pulse is indicated beside each record. The first point of the 'on' and 'off' transients has been removed. Base lines have been subtracted as in Fig. 3*Ac*. Spaces have been inserted in traces *d* and *e* so that the 'off' transients line up with the records above. *B*, difference between trace at left and trace *Aa* scaled according to the pulse amplitude. Thus *Bb* is given by *Ab* minus (3/2)*Aa*, *Bc* = *Ac* − (2)*Aa*, etc. The increase in noise from *b* to *e* is due to scaling *Aa* by progressively larger amounts. The two arrows mark the 'on' and 'off' of the pulse. Note change in gain from *A* to *B*. Same experiment as Fig. 3, average of four runs.

The magnitude of the 'off' currents in Fig. 6*A* also increased as the pulse was made more positive but the rate constants remained unchanged as might be expected since the 'off' step returned to the same holding potential in each case.

The records in Fig. 6*A* represent the average of four runs. Fig. 6*B*

shows the results of the first run. Apart from being noisier these traces resemble those in Fig. 6*A* except for the last one, +67 mV. Fig. 6*Bg* shows a rapid conductance change, probably due to delayed rectification, which is considerably more marked than the early change in Fig. 6*Ag*. This conductance change diminished in size during the experiment and by run 4 it was totally absent. Concomitantly, the charge movement at each voltage increased somewhat during the experiment (see column 4 of Table 1, fibre 10.2).

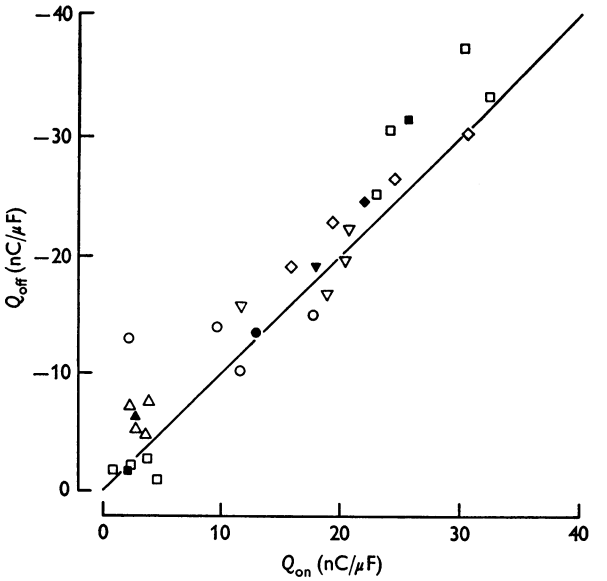

Fig. 8. Equality of 'on' and 'off' areas at different test potentials. The time integral of the transient component of ΔV(test-control) for the 'off' of a pulse is plotted against that measured for the 'on'. Areas determined from the average of four runs, Fig. 6*A*, are shown as filled symbols. Each individual run, such as Fig. 6*B*, is shown as an open symbol. □, ■, −60 mV; △, ▲, −50 mV; ○, ●, −40 mV; ▽, ▼, −30 mV; ◇, ◆, −11 mV; □, ■, 18 mV. The line is drawn at an angle of 45° and represents $Q_{off} = -Q_{on}$. Same experiment as Fig. 3.

Comparison of 'on' and 'off' areas

Schneider & Chandler (1973) showed that the amount of charge which moves during the pulse 'on' (Q_{on}) is equal to the absolute amount which moves during the pulse 'off' (Q_{off}). Fig. 8, which is similar to their Fig. 3*A*, supports this conclusion. The open symbols were obtained from analyses of single ΔV(test-control) records as shown in Fig. 6*B*, whereas the filled symbols were obtained using four averaged ΔV runs (Fig. 6*A*). There are no data points for +67 mV since the 'on' area could not be accurately

determined. The conductance change in the first three runs prevented a clear resolution of the charge movement.

To a good first approximation Fig. 8 supports the notion that $Q_{off} = -Q_{on}$. One must bear in mind, however, that the first point of each transient is somewhat arbitrary as discussed in connexion with Fig. 5. At 18 mV the first two points of each transient were out of range and so were set equal to the third, thereby introducing more uncertainty into the estimates of area. The general conclusion is that Q_{on} and Q_{off} are very nearly the same value although it is impossible to rule out a small difference.

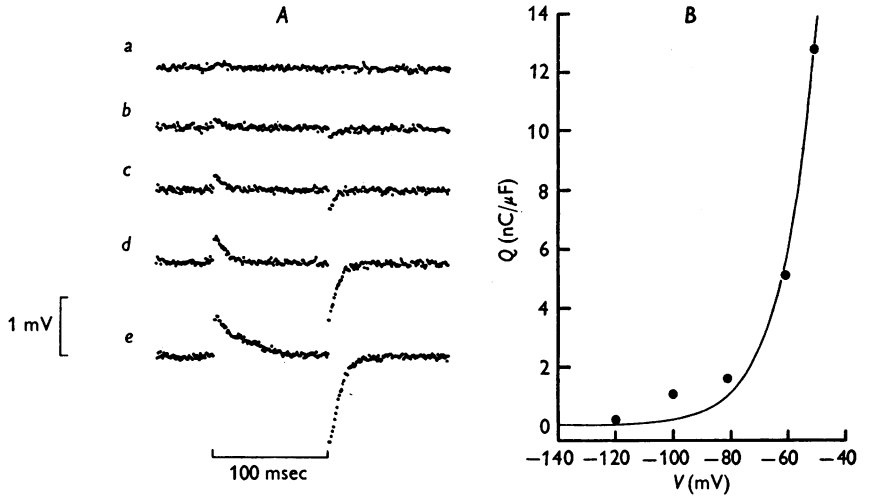

Fig. 9. Charge movement at negative potentials. *A*, ΔV(test-control) records where the test was a 29 mV pulse superimposed on a conditioning prepulse to −149 mV (*a*), −130 (*b*), −110 (*c*), −90 (*d*) or −80 (*e*). The control pulse was the same magnitude with a prepulse to −169 mV. Average of eight traces. *B*, average value of 'on' and 'off' areas from traces in *A*, plotted as a function of voltage V_1 during the positive pulse of the test. The continuous curve, drawn proportional to exp (V/12 mV), represents the best fit for an exponential function. Electrode spacing l = 191 μm, l' = 19 μm. Cable measurements gave λ = 0·0852 cm, r_i = 10·51 MΩ/cm, c_m = 0·2303 μF/cm so that 1 mV on ΔV represents 0·174 μA/cm (eqn. (1)) or 0·758 μA/μF. Fibre 18.13, 1·4° C. Initial resting potential −91 mV, holding potential −90 mV.

Charge movement at highly negative potentials

The experiments thus far suggest that charge movements of the type shown in the traces in Fig. 6 are not seen if the potential is restricted to values more negative than −80 mV. In Fig. 7 it was shown that between −150 and −80 mV the capacitative component behaved in an essentially

linear fashion, so that ΔV(test-control) would be small if both test and control voltages were in the range -150 to -80 mV.

This point was examined more carefully in another experiment using higher gain and more records for signal averaging. The relative absence of charge movement for $V < -80$ mV and its marked appearance at more positive voltages is shown in Fig. 9. The traces in part *A* show ΔV(test-control). The test was superimposed on a conditioning prepulse which varied from -149 (trace *a*) to -80 mV (trace *e*); the control was superimposed on a prepulse to -169 mV. The amplitude of the positive pulse was always 29 mV. Trace *a* shows essentially no charge movement, *b* and *c* show small amounts, and *d* and *e* show progressively larger amounts.

Fig. 9*B* shows the amount of charge as a function of membrane potential during the positive test pulse. The continuous curve, rather arbitrarily chosen, is proportional to $\exp(V/12$ mV). It provides a good fit except for the data points -80 and -100 mV (see p. 280). Since the deviations are small, about 1 nC/μF, little harm is done by assuming that the charge movement is absent for $V < -100$ mV.

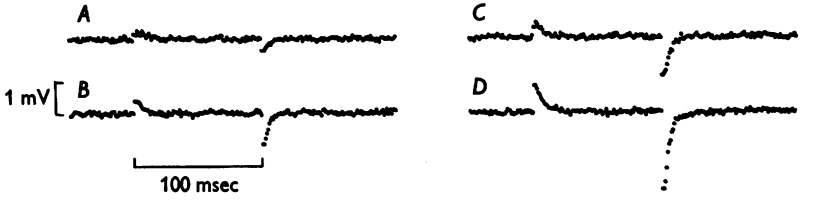

Fig. 10. Traces used to estimate charge distribution at the holding potential. Each trace is the average of four runs. In trace *A*, test = (-80, -60) and control = (-100, -80); *B*, test = (-100, -60) and control = (-140, -100); *C*, test = (-80, -50) and control = (-110, -80); *D*, test = (-100, -50) and control = (-150, -100). The notation (V_a, V_b) means that the membrane potential was V_a during the conditioning prepulse and V_b during the positive pulse. Trace *A* is the same as Fig. 6*Aa*, *C* the same as Fig. 6*Ab*. Same experiment as Fig. 3.

Charge distribution at the holding potential

The finding that the 'on' and 'off' areas of the charge movement are approximately equal (Fig. 8) and that the magnitude depends on potential suggests that there is an underlying relationship between charge distribution and membrane voltage, $Q(V)$. Since there is practically no charge movement for $V < -100$ mV, $Q(V)$ for $V < -100$ mV is approximately constant and may be taken arbitrarily as zero. In most experiments the holding potential (HP) was -80 mV with a corresponding value of approximately 1 nC/μF for $Q(HP)$ (Fig. 9).

Fig. 10 illustrates the method usually used to determine $Q(HP)$. Trace *A*

shows ΔV(test-control) where the test ΔV corresponds to V_1 changing from -80 to -60 mV during the positive pulse. This can be abbreviated $(-80, -60)$. The control record corresponds to $(-100, -80)$. The difference record Fig. 10*A*, ΔV(test-control), should yield $[Q(-60)-Q(-80)]-[Q(-80)-Q(-100)]$ as charge moved during pulse 'on'. Since $Q(-100) \doteqdot 0$, the difference is equal to $Q(-60)-2Q(-80)$.

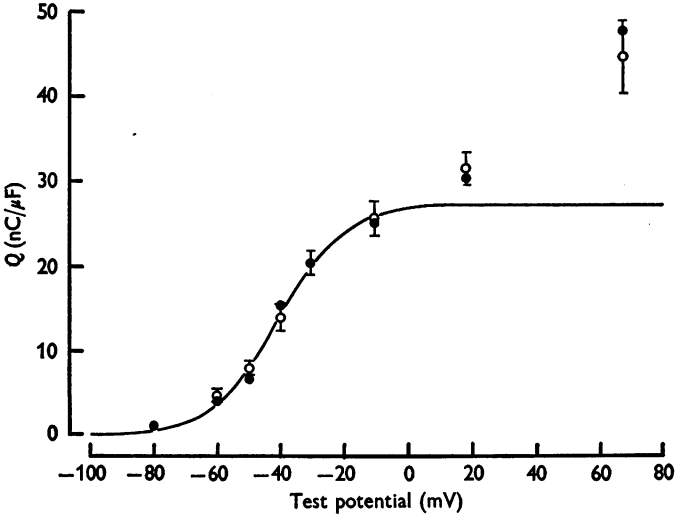

Fig. 11. Voltage dependence of charge movement. Data points represent measurements of the time integral of charge movement from the experiment in Fig. 6, corrected for $Q(-80) = 1{\cdot}07$ nC/μF as determined from Fig. 10. ●, mean of 'on' and 'off' determinations of the average of four runs, Fig. 6*A*. ○, mean of the four 'on' and four 'off' determinations of individual differences from each run. The first run is shown in Fig. 6*B*. The vertical bars indicate ± 1 S.E. of mean for the analysis of the individual runs. The rightmost points, $V = +67$ mV, are based on the 'off' areas alone. The curve was drawn according to eqn. (9) which was fitted to the open circles more negative than 0 mV. The best fit parameters were $\bar{V} = -41{\cdot}0$ mV, $k = 10{\cdot}4$ mV, $Q_{max} = 27{\cdot}4$ nC/μF. Same experiment as Fig. 3.

Trace 10*B* shows ΔV(test-control) where test $= (-100, -60)$ and control $= (-140, -100)$. In this case the 'on' area is simply $Q(-60)$. The average area of 'on' and 'off' in *B* is 3·35 nC/μF and in *A* is 1·96 nC/μF. The difference, 1·39 nC/μF, represents twice $Q(-80)$.

Traces 10*C* and *D* show the procedure repeated using a pulse to -50 mV. In this case the area associated with *C*, $Q(-50)-2Q(-80)$, was 4·58 nC/μF; from *D*, $Q(-50) = 7{\cdot}45$ nC/μF. The difference of 2·87 nC/μF gives $2Q(-80)$. The average value for $Q(-80)$ from the two estimates is 1·07 nC/μF. In experiments on four other fibres values for $Q(-80)$ ranged from 0 to 1·62 nC/μF.

Charge distribution vs. voltage

Fig. 11 shows $Q(V)$ *vs.* V analysed from the experiment in Fig. 6. The open circles, except for the rightmost point, are the average of eight numbers, the 'on' and 'off' areas determined from the single differences in each of the four runs. The rightmost point is based on 'off' area alone; the fast time course of the charge movement and the large conductance change during the pulse prevented an accurate estimate of the 'on' area. The vertical lines indicate ± 1 S.E. of mean.

The filled circles were obtained in a manner similar to the open ones except that traces of the average of four runs were used. As expected, the filled and open circles are in good agreement.

The theoretical curve was drawn according to a relatively simple scheme which describes the main properties of the charge distribution (Schneider & Chandler, 1973). It is assumed that a charged molecule or part of a molecule, confined to the membrane, is free to move between two locations which sense different proportions of the membrane potential. At rest most of the particles would be in position 1; on depolarization they would tend to move into position 2. There would be some intermediate voltage, call it $\bar{V}$, at which the steady-state distribution for positions 1 and 2 would be equal. An essential feature of the model is that when the voltage across the membrane changes from $\bar{V}$ to V, the potential difference between 1 and 2 changes by $A(V-\bar{V})$; A is a constant factor independent of potential.

If f_1 is the probability that position 1 is occupied, f_2 is the probability for position 2, and z is the valence, the Boltzmann relation gives in the steady state

$$f_1/f_2 = \exp[-(V-\bar{V})/k], \tag{6}$$

where k is the absolute value of RT/AzF. R is the gas constant, T is temperature and F is Faraday's constant. The requirement that $f_1+f_2 = 1$ allows eqn. (6) to be solved for f_2 to give

$$f_2 = 1/[1+\exp-(V-\bar{V})/k]. \tag{7}$$

If the total amount of observable charge is denoted by Q_{max} then $Q(V)$, the amount in position 2, is given by

$$Q(V) = f_2 Q_{max} \tag{8}$$

or

$$Q(V) = Q_{max}/[1+\exp-(V-\bar{V})/k]. \tag{9}$$

The continuous curve in Fig. 11 is drawn according to eqn. (9) and values of Q_{max}, $\bar{V}$ and k which give a best fit to the open circles.

In doing the fit only data points to the left of $V = 0$ were used. The main reason for not using the most positive two points was the presence

of conductance changes during the pulse (Fig. 6), so that for large depolarizations the early transient currents which we associate with charge movement might include an ionic component. An inward ionic current tail present on the 'off', for example, could explain why the 'off' area for 18 mV is larger than the 'on' area by about 20 % (see Fig. 8). The data points at $V = 67$ mV, associated with a larger conductance change and based entirely on the 'off', may be in substantial error.

Fig. 12 shows data from another experiment on a fibre from the same muscle, with a plateau more pronounced than in the previous Figure.

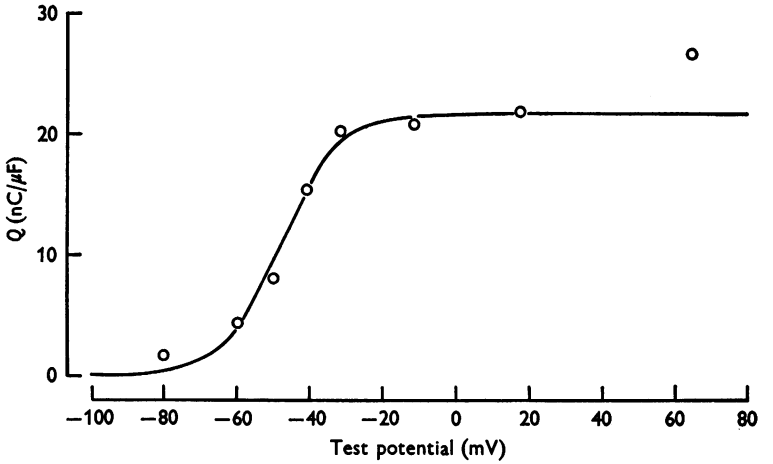

Fig. 12. Voltage dependence of charge movement. Symbols represent the mean of 'on' and 'off' areas, corrected for $Q(-80)$, signal average of two runs. The curve was fitted to data points more negative than 0 mV using eqn. (9); $\bar{V} = -47{\cdot}7$ mV, $k = 8{\cdot}0$ mV, $Q_{max} = 21{\cdot}5$ nC/μF. The point at 65 mV represents the 'off' transient only. Electrode spacing $l = 186$ μm, $l' = 19$ μm. From cable analysis $\lambda = 0{\cdot}0920$ cm, $r_i = 7{\cdot}69$ MΩ/cm, $c_m = 0{\cdot}258$ μF/cm. Fibre 10.5 (from same muscle as 10.2), 0·9° C. Initial resting potential −70 mV, holding potential −80 mV.

Table 1 gives the values of $\bar{V}$, k and Q_{max} for six fibres. Areas were measured on signal averaged traces and for fibre 10.2 on individual traces as well. There is considerable variability in these parameters. The average value of $\bar{V}$ was $-44{\cdot}1$ mV. The average of 7·8 mV for k gives a value of 3 for $|Az|$. If A were unity, i.e. if the charged particle traversed the entire membrane potential in moving from one position to the other, the valence z would have magnitude 3.

The average value of 24·5 nC/μF for Q_{max} corresponds to $15{\cdot}3 \times 10^{10}$ electronic charges per μF or, using the value of 3 for $|Az|$, $5{\cdot}1 \times 10^{10}$ charged groups per μF. If one takes the value of specific membrane capacitance to be 0·9 μF/cm^2 (Schneider, 1970; Hodgkin & Nakajima,

TABLE 1. Best fit parameters for charge *vs.* voltage

(1) Fibre	(2) $\bar{V}$ (mV)	(3) k (mV)	(4) Q_{max} (nC/μF)
10.2 (4)	−41·0	10·4	27·4
	(−43·6)	(9·4)	(19·1)
	(−39·5)	(8·1)	(23·1)
	(−40·7)	(9·1)	(28·1)
	(−38·7)	(9·7)	(32·9)
10.5 (2)	−47·7	8·0	21·5
11.1 (4)	−38·0	7·2	22·1
11.2 (1)	−32·4	5·2	22·0
18.13 (4)	−54·5	8·1	31·9
18.14 (2)	−51·2	7·7	22·1
Average ± S.E. of mean	−44·1 ± 3·4	7·8 ± 0·7	24·5 ± 1·7

Column (1) gives fibre reference and in parentheses the number of runs signal averaged. Columns (2)–(4) give values of parameters in eqn. (9) determined by a least-squares fit. The numbers in parentheses following fibre 10.2 were determined from the four individual runs and are listed in order. These values were not included in calculating the average values from the six fibres. The holding potential was −80 mV except for fibre 18.13 which was held at −90 mV. The value of k for this fibre, 8·1 mV, should be compared with the value of 12 mV for an e-fold change used in Fig. 9*B*, same fibre but different experimental protocol. Electrode spacing l varied from 186 to 195 μm, temperature 0·3–1·4° C.

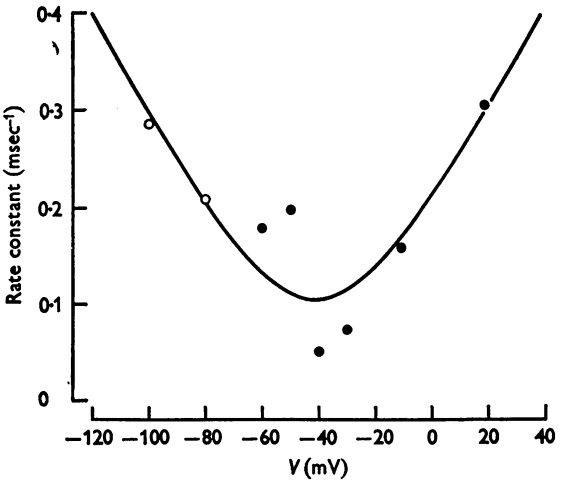

Fig. 13. Rate constants as a function of voltage. ○, average values obtained from 'off' measurements. The seven values at −80 mV had an average value of 0·208 msec^{-1} (range 0·173–0·249). The two values at −100 mV were 0·309 and 0·261 msec^{-1}. ●, values obtained from 'on' measurements. The curve shows the rate constant $(\alpha+\beta)$ calculated according to eqns. (11) and (12). Same experiment as Fig. 3.

1972) the density of charged groups is about 459/μm^2 averaged over surface and tubular membranes. If the groups are present only in the T-system the density would be 500–600/μm^2.

Kinetics of charge movement

Values for rate constants in the experiment in Figs. 6 and 11 are plotted in Fig. 13. Each rate constant was determined by fitting eqn. (5) to a record of ΔV(test-control) beginning 4–10 msec after the 'on' or 'off' of the voltage pulse. The first point used for the fit, individually selected for each trace, was chosen after the initial delay so that the fitted portion of the ΔV(test-control) trace was essentially exponential.

In order to find a theoretical fit to the data in Fig. 13, it was assumed that f_2 acts like a Hodgkin–Huxley (1952) variable, namely

$$df_2/dt = \alpha(1-f_2) - \beta f_2, \tag{10}$$

where α and β are functions only of voltage. The over-all rate constant is given by $\alpha+\beta$. The individual rate constants α and β were chosen to be symmetrical about $\bar{V}$ and to follow constant-field (Goldman, 1943) type voltage dependence. On this basis

$$\alpha = \frac{0{\cdot}053(V-\bar{V})/k}{1-\exp-(V-\bar{V})/k}, \tag{11}$$

$$\beta = \frac{0{\cdot}053(-V+\bar{V})/k}{1-\exp(V-\bar{V})/k}. \tag{12}$$

The values for $\bar{V}$ and k were taken from Table 1. The only adjusted parameter, the factor 0·053 msec^{-1}, was obtained by a least-squares fit. The curve in Fig. 13 gives a plot of the over-all rate constant ($\alpha+\beta$).

The open circles at -80 and -100 mV lie on the curve as do the filled circles at -11 and $+18$ mV. The middle four points do not fall on the curve. The two left-most ones, -60 and -50 mV, were obtained from traces *Aa* and *Ab* in Fig. 6. The charge movement transients were extremely small so that the determinations of the rate constants are considered unreliable. The two points at -40 and -30, from traces *Ac* and *Ad* in Fig. 6, are considered to be more reliable and indicate that eqns. (11) and (12) should be taken as only initial approximations. The point which does seem clear is that the curve of rate constant *vs.* voltage is U-shaped and approximately symmetrical about $\bar{V}$. Similar behaviour was shown in five other experiments.

Deviations from the simple model

The model used for fitting data assumes that the charge can occupy only one of two positions (eqns. 6–9) and that transitions obey first order

kinetics (eqn. 10). Although this simple scheme provides an adequate description of many of the results it fails in some respects. For example, Adrian and Almers (Almers, 1975) have shown that the rate constant for an intermediate depolarization can be changed by applying a strong conditioning depolarization. Eqn. (10), on the other hand, predicts that the rate constant should be independent of the initial voltage.

There are also indications in our experiments that simple first order behaviour is not observed. For example, many of the traces in Fig. 6*A* show a delay in the 'on' and 'off' responses so that the transients depart from a single exponential as required by eqn. (10).

If the charge movement process obeys first order kinetics, but is located in the tubules, delays comparable to those in Fig. 6*A* might be attributed to the time required to charge the tubular membranes. If this explanation were correct and if, in addition, α and β were symmetrical about $\bar{V}$, changes in potential symmetrical about $\bar{V}$ should give symmetrical ΔV responses. In Fig. 6*Ae* the test potential (-11 mV) and the holding potential (-80 mV) are almost equally spaced about $\bar{V}$ (-41 mV). The rate constants, plotted in Fig. 13, are nearly equal so that the 'on' and 'off' responses should be almost symmetrical in appearance. This is true to a first approximation.

In one experiment, however, this symmetry was markedly absent. Fig. 14*A* shows ΔV(test-control) records for different test potentials. Traces *c* to *f* show relatively large delays for the 'on' with smaller delays for the 'off' transients. Records of V_1(test-control) gave zero difference as illustrated in Fig. 14*B*. Thus the delays in the ΔV transients cannot be attributed to failure of the clamp to provide equally square test and control pulses.

In this experiment the holding potential was -90 mV and $\bar{V}$ was $-54{\cdot}5$ mV so that the pulse to -13 mV, record *f*, satisfies the criterion that the voltage swing is approximately symmetrical about $\bar{V}$. The ΔV trace is clearly asymmetrical, there being considerable delay for the 'on' and very little delay for the 'off'. The rate constants of the final exponential decay were nearly equal, as expected, with values of 0·099 msec^{-1} for -13 mV and 0·088 msec^{-1} for -90 mV.

Determination of passive properties of the T-system

It seems clear that the simple notion, namely that charge movements obey first order kinetics with a fixed tubular delay, cannot provide a complete description of the data. None the less, there remains the possibility that passive tubular properties account for part of the delay, making it of interest to analyse the passive electrical properties of the T-system. For this purpose pulses of ± 10 mV were applied from the holding

potential using voltage V_2 for feed-back control, as described in Methods. The space constant λ and product $r_1 c_m$ were determined as outlined in Methods. Using these values the time course of ΔV was fitted according to a Falk & Fatt (1964) equivalent circuit for the surface and tubular membranes (Fig. 18 and eqn. (13A)). Two parameters, the tubular time constant ($= r_s c_T$) and the ratio of surface to total capacitance ($= c_m'/c_m$ where $c_m = c_m' + c_T$), were adjusted to give a best least-squares fit.

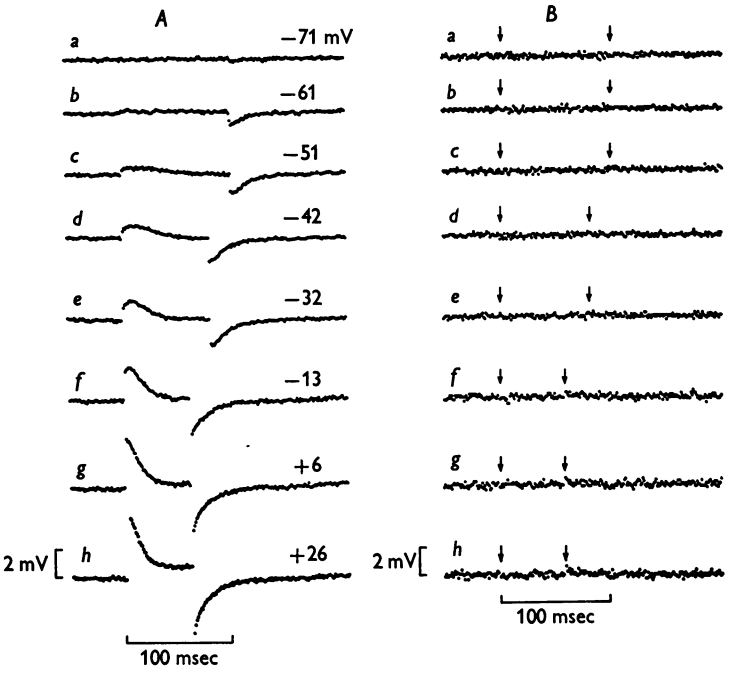

Fig. 14. ΔV(test-control) and V_1(test-control) at different voltages. A, ΔV(test-control) at different test potentials as indicated beside each record. B, V_1(test-control) associated with the records in A. Arrows mark pulse 'on' and 'off'. Average of four runs carried out in the same manner as the experiment in Fig. 6. Fibre 18.13, same as Fig. 9.

Although a distributed model for the T-system is probably more realistic than the lumped model (Schneider, 1970; Valdiosera, Clausen & Eisenberg, 1974), the lumped model is easier to handle mathematically and provides a description which is adequate for the present purposes.

Table 2 gives the results of the analysis carried out on the six fibres listed in Table 1. Columns (2), (4), (5) and (6) give values for four independent parameters which describe the Falk and Fatt equivalent circuit. The average value for λ, 0·0914 cm, is in close agreement with the value of 0·090 cm given by Adrian *et al.* (1970 *a*) for Ringer + 350 mM sucrose at

3° C. Column (6) gives values for the proportion of fibre capacitance ascribed to the surface, c'_m/c_m. The average value, 0·33, is exactly equal to the value reported by Valdiosera *et al.* (1974) who used a slightly less hypertonic solution (350 mM added sucrose) and worked at 22° C. The average value of tubular time constant, 2·28 msec, is also similar to their value of 2·77 msec. Values in isosmotic Ringer solution are smaller, 1·35 msec (Falk & Fatt, 1964), 0·72 msec (Schneider, 1970) and 0·60 msec (Valdiosera *et al.* 1974).

TABLE 2. Parameters for the Falk and Fatt equivalent circuit

(1) Fibre	(2) λ (cm)	(3) r_i (MΩ/cm)	(4) $r_i c_m$ (sec/cm²)	(5) $r_s c_T$ (msec)	(6) c'_m/c_m
10.2	0·0831	10·62	2·44	1·50	0·36
10.5	0·0920	7·69	1·98	2·20	0·40
11.1	0·0956	16·61	2·72	1·96	0·29
11.2	0·0749	20·54	2·44	2·03	0·26
18.13	0·0852	10·51	2·42	3·04	0·37
18.14	0·1178	4·45	2·24	2·95	0·31
Average ± S.E. of mean	0·0914 ± 0·0060		2·37 ± 0·10	2·28 ± 0·25	0·33 ± 0·02

Values in columns (2)–(4) were obtained from cable analysis as described in Methods. Columns (5) and (6) give parameters obtained by fitting eqn. (13A) in the Appendix to the 'on' part of the transient associated with steps of ± 10 mV, using values in columns (2) and (4) as constraints. Since each experimental point represents an average value over a 1 msec interval, eqn. (13A) was evaluated at successive points 50 μsec apart and the integral over 1 msec was obtained using a trapezoidal approximation. A 50 μsec delay was introduced to compensate for the 40 μsec delay on the command pulse and the 8 μsec delay introduced by the high frequency filter. These account for most of the delays when V_2 is used for voltage control, since there is practically no delay in V_2 following a ± 10 mV command pulse rounded with a 40 μsec time constant. In any event the effect of introducing the 50 μsec delay was small; it increased the average values of $r_s c_T$ by 0·1 msec and of c'_m/c_m by 0·04 over the values with no delay.

In the present study the smallest value of tubular time constant, 1·50 msec, was associated with fibre 10.2. Records of charge movement transients from this fibre (Fig. 6) showed less delay than records from the other fibres in Table 1. The greatest delay was seen in fibre 18.13 (Fig. 14) which gave the largest value for the time constant, 3·04 msec. The other four fibres in Table 2 showed delays of intermediate magnitude. Although the results to date are suggestive of a correlation between the delay in the charge movement transient and the tubular time constant, more experiments are needed to establish whether a definite relationship does, in fact, exist.

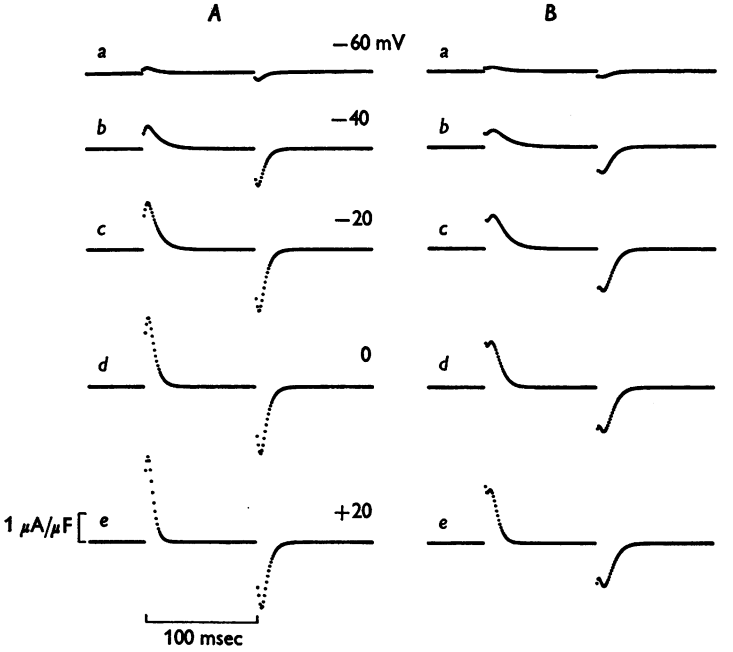

Fig. 15. Effect of tubular delay on the shape of calculated membrane current (test-control) records. The calculations were based on the equivalent circuit shown in Fig. 18 using $c'_m/(c'_m + c_T) = 0{\cdot}36$ and $r_s c_T = 1{\cdot}5$ msec (A) or 3·04 msec (B). The density of charged groups was considered to be uniform with respect to c'_m and c_T with a value of 27·4 nC/μF. The kinetics of charge movement are described by eqns. (8) and (10)–(12) with $\bar{V} = -41{\cdot}0$ mV, $k = 10{\cdot}4$ mV. For the calculations a step of potential was considered to be applied across the circuit in Fig. 18 with an additional charge movement element in parallel with each capacitance. The tubular currents were calculated using a conventional fourth-order Runge–Kutta method, the surface currents from the exponential solution of eqn. (10). The test and control calculations were based on the same pulse/prepulse arrangement as used in the experiments. Each point is the average value over a 1 msec interval: the first point of each 'on' and 'off' transient has been omitted.

Effect of tubular delay on calculated charge movement currents

In order to assess the effect that a tubular delay would impose on the shape of the charge movement transient, calculations were carried out using a lumped Falk & Fatt (1964) model for the surface plus tubular membranes (Fig. 18). The charged groups were assumed to be uniformly distributed according to membrane capacitance and to be electrically in parallel with the capacitative elements c'_m and c_T. The kinetics of charge movement were assumed to be first order so that eqns. (8), (10), (11) and (12) apply. Values of $\bar{V}$, k and Q_{max} were taken from fibre 10.2 (Table 1).

Fig. 15*A* shows theoretical calculations of membrane current, analogous to ΔV(test-control), using the value for the tubular time constant $r_s c_T$ which was measured on fibre 10.2 (Fig. 6), 1·5 msec. Delays of a few msec are present in every record. Fig. 15*B* shows more pronounced delays, calculated using $r_s c_T$ = 3·04 msec as obtained from fibre 18.13 (Fig. 14). In addition, the larger value of $r_s c_T$ has produced an apparent increase in the time constant associated with the final decline of the transient current.

In comparing the transient currents in the experimental records in Fig. 6*A* with the calculations in Fig. 15*A* several discrepancies are apparent. The calculated 'on' and 'off' records for moderate depolarizations tend to be more symmetrical than the experimentally observed currents. Thus the amplitude of the peak transient current during pulse 'on' in trace *c* of Fig. 6*A* is about 0·4 times the peak during pulse 'off' whereas in trace *b* of Fig. 15*A* the ratio is 0·6. This difference is related to the fact that the constant field functions used to describe α and β (see Fig. 13) give a higher value for the rate constant than was observed around −40 mV. Another difference is that the calculated delays in Fig. 15*A* are somewhat more pronounced than the experimental ones in Fig. 6*A*.

The traces in Fig. 15*B* show more delay than those in 15*A* and in some respects resemble records in Fig. 14*A*. The main difference of concern between the two sets of records is the relative lack of a delay in the experimental 'off' transient following a strong depolarization.

The theoretical curves in Fig. 15 should be considered as rough approximations to the actual situation. In a proper analysis a distributed model for the tubular system would be used and any difference in density of charged groups between surface and tubular membranes would be taken into account. One would expect, for example, that the rather clear temporal separation of surface and tubular current components, indicated in Fig. 15*Bd* and *Be* as an early dip in the records, would give way to a smoother response using a distributed model for the T-system. The main conclusion from the calculations is that if the charge is located in the T-system then the time course of the current transients will be distorted, thereby making a quantitative analysis of the kinetics of charge movement difficult.

As mentioned earlier, asymmetries of the type seen in trace *f* of Fig. 14*A*, when $\bar{V}$ is midway between the holding and the test potentials, cannot be explained by first order kinetics for Q and a fixed tubular delay. To do that one needs to assume a more complicated kinetic scheme for charge or possibly to invoke an effect of voltage or current flow on r_s.

DISCUSSION

The three most important electrical properties of the charge movement currents are (1) that the total charge which moves during pulse 'on' is equal but opposite to that which moves during pulse 'off', (2) that the steady-state curve relating charge to membrane potential is a saturating sigmoid function and (3) that the rate constants for both 'on' and 'off' transients are strongly voltage dependent. The first property, the equality of charge, holds when the amount of charge is varied by changing either the duration (Schneider & Chandler, 1973) or magnitude (Schneider & Chandler, 1973; this paper) of the pulse, or by slow inactivation during maintained depolarization (Chandler, Rakowski & Schneider, 1976). These properties, as well as certain kinetic features (Schneider & Chandler, 1973), make it unlikely that the currents are carried by intra- or extracellular ions passing through channels in the membrane. Rather, the currents most likely represent the movement of particles which are confined to the membrane itself, either dipoles which reorient or charged groups which move in response to changes in the membrane electric field. Alternative explanations should be considered, however, and some of these will be discussed below.

A. *Non-linear properties of* r_1

Since with the three micro-electrode technique the measured signal used to estimate current, ΔV, is proportional to the product $r_1 i_m$ (eqn. (1)), it is natural to wonder whether the small transients in ΔV are due to non-ohmic behaviour of r_1 rather than non-linearities in membrane properties. This seems unlikely since r_1 is independent both of frequency, up to 10 kHz (Mobley, Leung & Eisenberg, 1974), and of d.c. membrane potential (Schneider & Chandler, 1976).

B. *Changes in membrane thickness with voltage*

When a potential difference is imposed across a capacitance a coulombic force attracts the oppositely charged plates, tending to decrease the distance of separation and thereby to increase the value of the capacitance. This effect, known as electrostriction, results in a capacitance *vs.* voltage curve that is U-shaped and symmetrical about $V = 0$. In the simplest case the curve is a parabola.

The muscle membrane also shows a voltage dependent capacitance owing to the non-linearities associated with the charge movement. At low frequencies this component is given simply by dQ/dV which, from eqn. (9), is seen to be bell-shaped, reaching a maximum of $Q_{max}/4k$ at $V = \bar{V}$ and approaching zero as V tends to $\pm\infty$. Thus the shape of the capacitance

vs. voltage curve associated with the charge movement is inconsistent with the mechanism being a change in membrane thickness due to electrostriction.

The time course of the ΔV transient is also inconsistent with electrostriction. To a very rough approximation on that basis the test ΔV trace in Fig. 3*Bb* should resemble trace 3*Ab* but scaled with respect to time by a constant factor. Instead, the fast components of the 'on' and 'off'

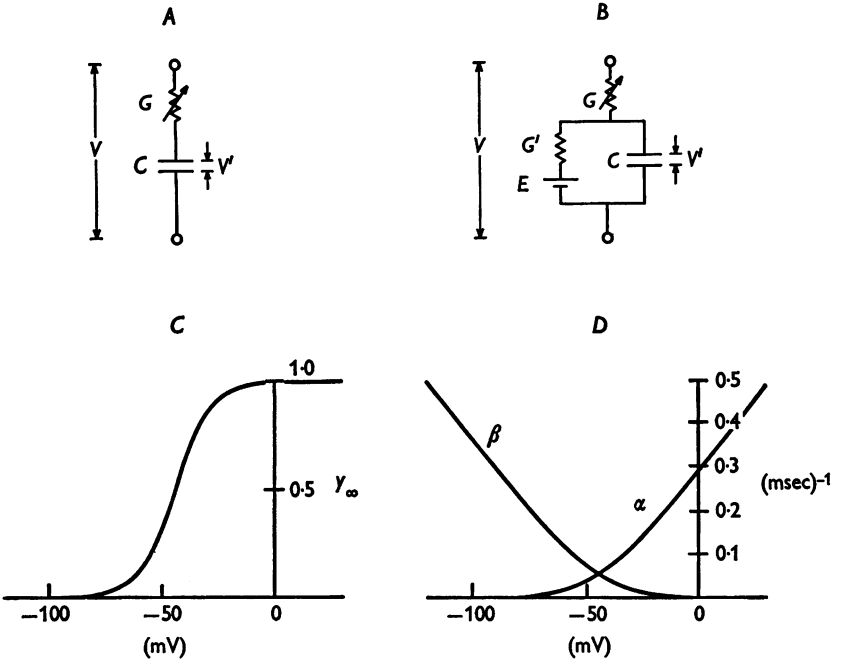

Fig. 16. *A* and *B*, electrical circuits in which *G* is a voltage dependent conductance; *G'*, *C* and *E* are constant. *C*, curve for $y_\infty[=\alpha/(\alpha+\beta)]$ and *D*, curves for α and β; these were calculated from eqns. (11) and (12) using $\bar{V} = -44$ mV, $k = 8$ mV (Table 1).

transients in Fig. 3*Ab* and *Bb* are about the same; the difference is the appearance in Fig. 3*Bb* of a separate slow component. This behaviour strongly suggests that the charge movement process lies electrically in parallel with the usual linear membrane capacitance, and it is processes of this type which will be considered in the following sections.

C. *Voltage dependent resistance in series with a portion of the T-system*

One might imagine that the electrical circuit shown in Fig. 16*A*, placed in parallel with the linear electrical properties of the membrane, might be able to reproduce the charge movement currents. *G* would be zero at

highly negative voltages and would increase at positive voltages. Physically this might correspond to a fraction of the tubular system being electrically closed off from the extracellular fluid at the resting potential but able to open up on depolarization. Three general types of voltage dependent properties will be considered for G.

(i) *G depends instantaneously on membrane potential.* In this case G is an instantaneous function of V, the total potential across the resistive and capacitative elements (Fig. 16*A*). The scheme, however, fails in two respects. First, if the voltage is taken from the holding potential V_{HP} to a value V sufficiently positive that charge movement currents are observed, the amount of charge associated with the 'on' transient, Q_{on}, would be

$$Q_{on} = C[V'(\infty) - V'(0)], \tag{13}$$

$$= C[V - V_{HP}]. \tag{14}$$

V' refers to the voltage across the capacitance (Fig. 16*A*) with 0 and ∞ denoting initial and final values. Accordingly Q_{on} would increase in proportion to $(V - V_{HP})$ rather than saturating at positive potentials (Figs. 11, 12).

The second difficulty concerns 'off' areas. Once V is brought back to V_{HP}, G would immediately return to a near zero value so that the time constant for current flow would become extremely long. The small, slowly changing currents would be taken for a slow drift in either the ionic currents or the base line, leaving zero for the estimate of 'off' area. Experimentally the 'off' area is as large as the 'on' (Fig. 8), with a relatively small time constant for the decay of the current (Fig. 13).

(ii) *G depends on membrane potential but with a delay.* In this case Q_{on} is still given by eqn. (14) so that the difficulty encountered in case (i) with explaining the saturating experimental curve for Q_{on} *vs.* voltage would remain. The values of 'off' areas are increased considerably over those in case (i) although not enough to bring the magnitudes of Q_{off} and Q_{on} into agreement. The linear relationship between Q_{on} *vs.* $(V - V_{HP})$ could be dealt with by assuming a voltage dependence for C, as well as G, but it is difficult to make the 'on' and 'off' areas agree and also to preserve the observed voltage dependence of the 'off' rate constant.

The basis for the statements concerning the discrepancy $|Q_{off}| < |Q_{on}|$ is an analysis of 'off' areas in which definite assumptions were made concerning the way in which G can change with V. G was assumed to be regulated by a Hodgkin–Huxley (1952) variable y,

$$G = yG_{max}, \tag{15}$$

$$dy/dt = \alpha(1-y) - \beta y. \tag{16}$$

The curves relating y_∞, α and β to voltage V across the network, taken from eqns. (11) and (12), are shown in Fig. 16*C* and *D*. Current was calculated according to

$$I = G(V - V'). \tag{17}$$

For a step change in voltage from V to V_{HP} eqns. (15) and (16) can be solved to give

$$G = G_{max}[y_\infty + (y_0 - y_\infty)\exp -(\alpha+\beta)t], \tag{18}$$

where y_0 and y_∞ are initial and final values of y. The time course of V', obtained by integrating

$$dV'/dt = G(V_{HP} - V')/C, \tag{19}$$

is given by

$$V' = V_{HP} - (V_{HP} - V)\exp\left\{-\frac{G_{max}}{C}\left[y_\infty t + \left(\frac{y_0 - y_\infty}{\alpha+\beta}\right)(1-\exp-(\alpha+\beta)t)\right]\right\}. \tag{20}$$

Since y_∞ at the holding potential is nearly zero eqn. (20) becomes for large times

$$V'(\infty) = V_{HP} - (V_{HP} - V)\exp\left\{-\frac{y_0 G_{max}/C}{(\alpha+\beta)}\right\}. \tag{21}$$

The charge associated with the 'off' transient, Q_{off}, is given by

$$Q_{off} = C[V'(\infty) - V], \tag{22}$$

$$= C[V_{HP} - V]\left[1 - \exp\left\{-\frac{y_0 G_{max}/C}{(\alpha+\beta)}\right\}\right]. \tag{23}$$

The consequences of eqns. (21) and (23) depend on the relative magnitudes of $(\alpha+\beta)$ and $y_0 G_{max}/C$. If $(\alpha+\beta)$ were very small compared with $y_0 G_{max}/C$, the exponential term in the equations would be zero. $V'(\infty)$ would equal V_{HP} and the magnitude of Q_{off} (eqn. 23) would be the same as Q_{on} (eqn. 14), in agreement with experiment. The time course of decay of V', determined from eqn. (20), would follow a single exponential with rate constant $y_0 G_{max}/C$. Since G would remain essentially constant during the transient, the current according to eqn. (17) would also follow a single exponential with the same rate constant $y_0 G_{max}/C$. Thus the time constant of the 'off' transient calculated using these assumptions would be a function of the 'on' voltage and would be independent of the 'off' voltage, in conflict with experimental observations.

To explain the voltage dependence of the 'off' rate constant (Fig. 13) it is necessary to make $y_0 G_{max}/C$ and $(\alpha+\beta)$ the same order of magnitude; at increasingly negative potentials the decline of y would become progressively more rapid and tend to dominate the $y_0 G_{max}/C$ rate constant. In the extreme case in which $(\alpha+\beta) \gg y_0 G_{max}/C$, V' would remain at V during the period when G shuts off so that eqn. (17) would reduce to a single exponential with rate constant $(\alpha+\beta)$.

Sample calculations using the curves in Fig. 16*D* for α and β and a value of 0·2 msec^{-1} for G_{max}/C gave approximately the correct voltage dependence for the decay of the 'off' current. At -80 mV the value of the exponential term in eqn. (23) is 0·44 and at -100 mV it is 0·58, indicating that Q_{off} would be 0·56 and 0·42 times Q_{on} in magnitude at these respective voltages. Thus, if this case is adjusted to give reasonable 'off' time constants it fails to reproduce the experimentally observed equality of 'on' and 'off' areas.

In the actual situation for the 'off' current, y_∞ would not be exactly zero, just very small. The current would consist of two components, a rapidly decaying one which would be similar to the case $y_\infty = 0$ and a more slowly decaying one which would eventually restore V' to V_{HP}. Experimentally, the second component would be relatively inconspicuous and therefore ignored in the determination to Q_{off}.

(iii) *G depends on the potential difference developed across itself.* Another possibility for the circuit in Fig. 16*A* is to assume that G depends not on total membrane potential V but on the potential developed across itself

$(V - V')$. This case is easy to dispense with. In the steady state the voltage across G is zero, independent of the value of V, so that the initial conditions for the control and test records would be identical. For experiments in which the same size voltage step was used for the control and the test, i.e. for depolarizations of up to 70 mV from the holding potential, the current records would be identical and ΔV(test-control) would equal zero at all times.

D. *Partial electrical shunt into the sarcoplasmic reticulum (S-R)*

Some of the difficulties encountered with the circuit in Fig. 16*A* are removed by the changes shown in Fig. 16*B*. Physically, G' and C could represent the conductance and capacitance of the S-R membrane, E its resting potential, and G a voltage dependent conductance connecting the T-system to the S-R. In this case G is determined by eqn. (15) and current by eqn. (17), where V' again denotes the voltage across C. In the steady state,

$$V' = \frac{(G/G')V + E}{(G/G') + 1}. \tag{24}$$

The maximum amount of charge movement, Q_{max}, corresponds to 0·2–0·4 times the charge associated with a 100 mV change in voltage across the capacitance of the tubular membranes, or 0·013–0·027 times the charge necessary to produce the same change in voltage across the S-R membranes, assuming the same specific capacitance for both tubular and S-R membranes and a value of 15 for the ratio of S-R : T-system membrane area (Peachey, 1965; Peachey & Schild, 1968). This indicates that the ratio G/G' is restricted to small values.

In the simplest scheme G and G' would be constants and the 'effective' capacitance of the circuit in Fig. 16*B* would be given by $CG^2/(G' + G)^2$ (cf. eqn. 15 in Adrian & Almers, 1974) which according to eqn. (15) equals $CG_{max}^2/(G' + G_{max})^2$ for $y = 1$. The range 0·013–0·027 for $G_{max}^2/(G' + G_{max})^2$ corresponds to $G_{max}/G' = 0{\cdot}13$–$0{\cdot}20$. The situation becomes complicated if G/G' is voltage dependent so that it is necessary to explore several specific cases, similar to those discussed for the circuit in Fig. 16*A*.

(i) *G depends instantaneously on membrane potential.* For a voltage step from V_0 to V, V' changes exponentially according to

$$V' = V'(\infty) + [V'(0) - V'(\infty)] \exp[-(G + G')t/C] \tag{25}$$

and from eqn. (17), the current also changes exponentially,

$$I = \frac{(V - E)GG'}{G + G'} + G[V'(\infty) - V'(0)] \exp[-(G + G')t/C]. \tag{26}$$

Some examples of currents calculated from this equation are shown in Fig. 17, thin lines. The 'on' transients can be as large as those observed experimentally but the direction is influenced by the value of E (compare A, B and C). The 'off' transients are negligible regardless of the value of E, showing clearly that this model will not work.

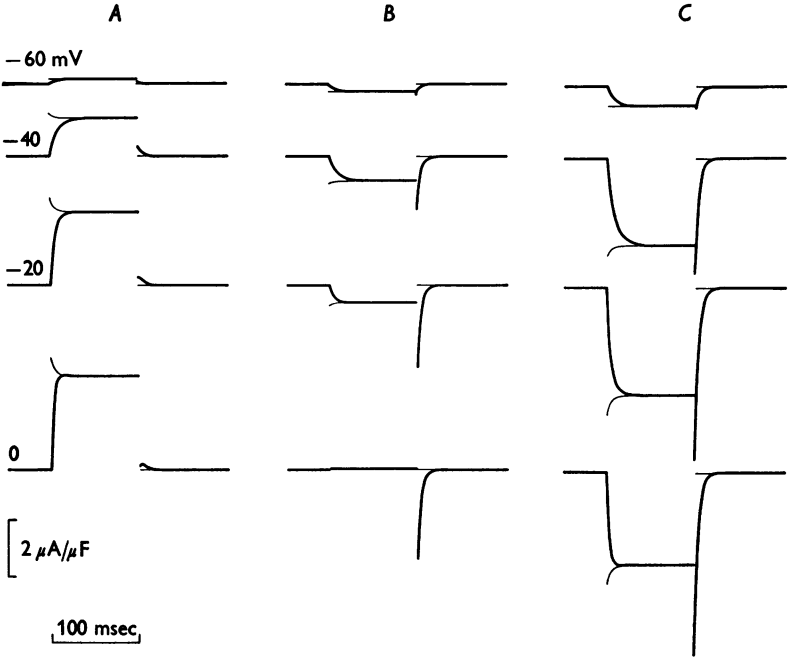

Fig. 17. Theoretical curves for current flow across circuit in Fig. 16B for different values of E. The currents have been normalized by dividing by C. The thin curves were calculated from eqn. (26) which assumes that G is an instantaneous function of V; the thick curves were calculated using a delay in G, eqns. (11), (12), (16), (27), (15), and (17). The circuit parameters were $G_{max}/G' = 0{\cdot}2$; $G'/C = 0{\cdot}2$ msec^{-1}; $E = -100$ mV (A), 0 mV (B), 100 mV (C). The holding potential was taken as -80 mV; pulse voltages were -60, -40, -20 and 0 mV as indicated. The holding current÷capacitance was 0·009 μA/μF in A, $-0{\cdot}035$ μA/μF in B, $-0{\cdot}079$ μA/μF in C.

(ii) *G depends on membrane potential but with a delay.* In this section G is assumed to be governed by eqn. (15), changes in y by eqn. (16). The curves in Fig. 16D show the rate constants α and β. In this situation it is necessary to use numerical methods to solve the equation for V',

$$dV'/dt = [yG_{max}(V - V') - G'(V' - E)]/C. \qquad (27)$$

Eqns. (16) and (27) were solved using a fourth order Runge–Kutta method (Romanelli, 1960) and currents were calculated using eqn. (17). The thick curves in Fig. 17 show some of the results. The currents have been

normalized by dividing by C referred to S-R membrane; current densities with respect to T-system membrane, using the assumptions given earlier, would be 15 times larger.

Fig. 17*A* shows the effects of the delay in G using $E = -100$ mV. The 'on' and 'off' transients are in the wrong direction, i.e. the transient component of the 'on' current is inward and the transient component of the 'off' is outward, and the areas are not in agreement.

As long as G/G' is small the properties of the transient currents are determined by G and E. For the smallest voltage, -60 mV, V' barely deviates from the value of E, -100 mV; at the holding potential $V' = -99{\cdot}96$ mV and during the pulse it changes to $-99{\cdot}07$ mV. The $(V-V')$ term is almost constant at the value $(V-E)$, changing from 39·96 to 39·07 mV, a deviation of at most 2·3 % from $(V-E) = 40$ mV. Thus, eqn. (17) can be replaced by the approximation

$$I \doteqdot G(V-E) \tag{28}$$

so that the area of the transient becomes

$$Q \doteqdot \frac{G(0)-G(\infty)}{\alpha+\beta}(V-E). \tag{29}$$

The values of G' and C do not enter at all.

At more positive potentials V' undergoes a greater change during the pulse. At $V = 0$ it becomes $-83{\cdot}39$ mV so that $(V-V') = 83{\cdot}39$ mV instead of $(V-E) = 100$ mV. The deviation is sufficiently small, however, that eqn. (28) may still be used to provide a rough estimate of the currents.

These arguments hold for other values of E so that eqns. (28) and (29) may be used as a qualitative guide in understanding parts *B* and *C* of Fig. 17. For $E = 0$ (Fig. 17*B*) the value of $(V-E)$ is negative for $V < 0$ so that the direction of the transients is correct. At $V = 0$, however, $(V-E) = 0$ so that the 'on' transient disappears although the 'off' transient is large. These records show that the value $E = 0$ does not work for two reasons: the area of the 'on' transient does not plateau with voltage and the 'on' and 'off' areas do not agree. The presence of an inward steady-state current during the pulse for $V < 0$ might also be considered an objection; this could in theory be balanced by an outward rectification of leakage current in the surface or tubular membrane.

The traces in Fig. 17*C*, $E = 100$ mV, also fail to duplicate the experimental results. The 'on' transients are outward but the areas do not produce a plateau; they reach a maximum between -40 and -20 mV and then tend towards zero as V approaches E. The reason is that for $V > -20$ mV the difference $G(\infty)-G(0)$ is essentially maximal and constant. According to eqn. (29) the area of the transient is then proportional

to $(E-V)/(\alpha+\beta)$, which decreases as V is made more positive. In addition, the 'on' and 'off' areas are not in agreement.

The defect with the plateau could probably be remedied by adjusting α and β so that y_∞ (Fig. 16*C*), and therefore $G(\infty)-G(0)$, would increase with voltage and would thereby offset the decrease in $(E-V)/(\alpha+\beta)$. If this were done to provide a plateau for Q_{on} *vs.* V, Q_{off} *vs.* V would not show a plateau. According to eqn. (29) the magnitude of Q_{off} would increase in proportion to $G(\infty)-G(0)$, since at V_{HP} the relation $(V-E)/(\alpha+\beta)$ would not vary.

The general conclusion from the calculations in Fig. 17 is that the areas 'on' and 'off' do not agree. This is not surprising since the areas are determined primarily by E, V and the properties of G. The process of charging and of discharging the capacitance C, which would demand equality of charge, plays a minor role in determining the transient current which flows through the entire circuit.

(iii) *G depends on the potential difference developed across itself.* Since the voltage across the capacitance C in Fig. 16*B* is roughly fixed at E, the potential across G is approximately $(V-E)$, the total voltage shifted by a constant amount. Therefore, the same objections given under (i) and (ii) apply.

E. *Rearrangements of dipoles or charges confined to the membrane phase*

The properties of the charge movement currents tend to rule out mechanisms (A) to (D) and leave (E) as the most likely possibility. In terms of function, a charge rearrangement of this type could play a role in giving a steep voltage dependence to some physiological process. In the original description of the charge movement (Schneider & Chandler, 1973) the suggestion was made that it might play a role in excitation-contraction coupling. A second possibility is that the currents gate potassium channels. These two possibilities seem to be the most plausible ones and they will be discussed further in the succeeding paper (Chandler *et al.* 1976). It is clear, however, that the currents do not gate sodium channels because the kinetics are too slow (Armstrong & Bezanilla, 1973, 1974; Keynes & Rojas, 1973, 1974).

A third possibility would be to suppose that the charged groups serve as a carrier for ions. For example, a membrane-confined carrier might combine with ions and be able to cross the membrane as a carrier-ion complex. The equality of 'on' and 'off' areas would place certain restrictions on the scheme, such as requiring that the valence state of the carrier or carrier-ion complex remain constant during a 100 msec pulse.

Additional complications

Several difficulties have already been mentioned. If the charge movement occurs in the T-system, then the delay in tubular potential following a voltage step at the surface will introduce a delay in the charge movement currents. A delay of this type would make a kinetic analysis of the charge transients difficult. In addition, the results of Adrian and Almers (Almers, 1975) and the asymmetry in record *f*, Fig. 14*A*, indicate that the kinetics of the charge movement process itself are neither first order nor symmetrical about $\bar{V}$. The rather simple relationship for Q *vs.* V (eqn. (9)), symmetrical about $\bar{V}$, is also most likely incorrect although our data are not sufficiently accurate to distinguish this model from a more complex one.

Finally, there is a second charge movement process in muscle, which we will call Charge 2, best seen with maintained depolarization which inactivates the first charge process (Chandler *et al.* 1976). The kinetics of Charge 2 were first studied by Adrian and Almers (Almers, 1975) who used fibres in hypertonic solution which were depolarized electrically. In other experiments fibres have been depolarized by isosmotic solutions containing high rubidium. These fibres show a capacitance which is weakly voltage dependent (Schneider & Chandler, 1976) and Charge 2 currents similar to those found by Adrian and Almers (Adrian, Chandler & Rakowski, 1976). The main difference between Charge 1 and 2, besides the fact that Charge 2 does not inactivate with maintained depolarization, is that Q *vs.* V for Charge 2 is 5–10 times broader than the curve for Charge 1. Since the curve for Charge 2 is roughly symmetrical about the holding potential, -80 mV, a 'control' and a 'test' ΔV trace in the present experiments would contain similar amounts of Charge 2 which would approximately cancel when subtracted. The only indication of Charge 2 in this paper is possibly the slight deviation of the points in Fig. 9*B*, obtained from traces 9*Ab* and 9*Ac*, from the exponential curve.

We thank Mr H. Fein and staff for help with design and construction of equipment and Dr R. W. Tsien for helpful discussion. Financial support was provided by the U.S. National Institutes of Health, grant NB-07474, and by the Muscular Dystrophy Associations of America, research fellowship to R.F.R.

APPENDIX

The aim of this section is to derive the time course of potential spread along a muscle fibre following a step in potential V_2 at $x = 2l$, using a lumped equivalent circuit for the surface and T-system membranes as shown in Fig. 18 (Falk & Fatt, 1964). The mathematical treatment is similar to the theory for chemical fluxes presented by Harris & Burn (1949).

The two partial differential equations which must be solved simultaneously are

$$\frac{\partial^2 V}{\partial x^2} = \frac{V}{\lambda^2} + r_i c'_m \frac{\partial V}{\partial t} + r_i c_T \frac{\partial V_T}{\partial t}, \tag{1A}$$

$$r_s c_T \frac{\partial V_T}{\partial t} = V - V_T, \tag{2A}$$

where V and V_T are the potentials across c'_m and c_T respectively.

For mathematical simplicity the time course for the 'off' response will be given first and then superposition will be used to evaluate the 'on' response. The boundary and initial conditions for the 'off' response are

(*a*) $\partial V/\partial x = 0$ at $x = 0$ for $t \geqslant 0$,

(*b*) $V = 0$ at $x = 2l$ for $t \geqslant 0$,

(*c*) V and $V_T = V_2 \dfrac{\cosh(x/\lambda)}{\cosh(2l/\lambda)}$ for $0 \leqslant x < 2l$ and $t = 0$.

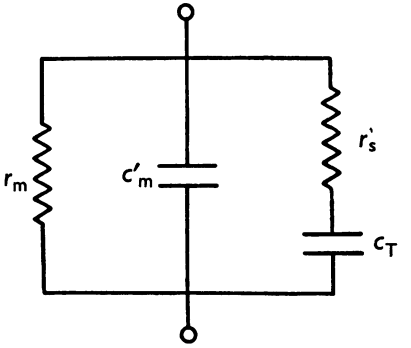

Fig. 18. Falk and Fatt lumped equivalent circuit for a 1 cm length of fibre. r_m = surface resistance; c'_m = surface capacitance; r_s = tubular resistance in series with c_T; c_T = tubular capacitance. The total membrane capacitance c_m is given by $c_m = c'_m + c_T$.

The general solution for eqns. (1A) and (2A) with conditions (*a*) to (*c*) is given by

$$V = \sum_{n=0}^{\infty} A_n \cos(\mu_n x)\phi_n(t), \tag{3A}$$

$$V_T = \sum_{n=0}^{\infty} A_n \cos(\mu_n x)\psi_n(t), \tag{4A}$$

where $\mu_n = \dfrac{1}{2l}\left(n + \dfrac{1}{2}\right)\pi$, $\phi_n(0) = \psi_n(0) = 1$, $\phi_n(\infty) = \psi_n(\infty) = 0$. The A_n satisfy

$$V_2 \frac{\cosh(x/\lambda)}{\cosh(2l/\lambda)} = \sum_{n=0}^{\infty} A_n \cos(\mu_n x), \tag{5A}$$

which gives $$A_n = (-1)^n \frac{V_2}{l} \frac{\mu_n}{(1/\lambda^2)+\mu_n{}^2}. \quad (6A)$$

The functions ϕ_n and ψ_n are determined by substituting eqns. (3A) and (4A) into (1A) and (2A). The result is

$$\phi_n = \frac{(1-r_s c_T q_n)p_n}{p_n-q_n} \exp(-q_n t) - \frac{(1-r_s c_T p_n)q_n}{p_n-q_n} \exp(-p_n t), \quad (7A)$$

$$\psi_n = \frac{p_n}{p_n-q_n} \exp(-q_n t) - \frac{q_n}{p_n-q_n} \exp(-p_n t), \quad (8A)$$

where $$p_n = \tfrac{1}{2}[F_n + \sqrt{(F_n^2 - G_n)}], \quad (9A)$$

$$q_n = \tfrac{1}{2}[F_n - \sqrt{(F_n^2 - G_n)}], \quad (10A)$$

$$F_n = \frac{1}{r_s c_m'} + \frac{1}{r_s c_T} + (\mu_n^3 + 1/\lambda^2) \frac{1}{r_i c_m'}, \quad (11A)$$

$$G_n = \frac{4}{r_i r_s c_m' c_T} (\mu_n{}^2 + 1/\lambda^2). \quad (12A)$$

The 'on' response following a step to V_2 at $x = 2l$ is given by the steady-state solution minus the 'off' response

$$V = V_2 \frac{\cosh(x/\lambda)}{\cosh(2l/\lambda)} - \sum_{n=0}^{\infty} A_n \cos(\mu_n x)\phi_n(t), \quad (13A)$$

where A_n, μ_n and $\phi_n(t)$ have the same values as above.

REFERENCES

ADRIAN, R. H. & ALMERS, W. (1974). Membrane capacity measurements on frog skeletal muscle in media of low ionic content. *J. Physiol.* **237**, 573–606.

ADRIAN, R. H., CHANDLER, W. K. & HODGKIN, A. L. (1969). The kinetics of mechanical activation in frog muscle. *J. Physiol.* **204**, 207–230.

ADRIAN, R. H., CHANDLER, W. K. & HODGKIN, A. L. (1970*a*). Voltage clamp experiments in striated muscle fibres. *J. Physiol.* **208**, 607–644.

ADRIAN, R. H., CHANDLER, W. K. & HODGKIN, A. L. (1970*b*). Slow changes in potassium permeability in skeletal muscle. *J. Physiol.* **208**, 645–668.

ADRIAN, R. H., CHANDLER, W. K. & RAKOWSKI, R. F. (1976). Charge movement and mechanical repriming in skeletal muscle. *J. Physiol.* **254**, 361–388.

ADRIAN, R. H. & FREYGANG, W. H. (1962). The potassium and chloride conductance of frog muscle membrane. *J. Physiol.* **163**, 61–103.

ALMERS, W. (1975). Observations on intramembrane charge movements in skeletal muscle. *Phil. Trans. R. Soc.* B **270**, 507–513.

ARMSTRONG, C. M. & BEZANILLA, F. (1973). Currents related to movement of the gating particles of the sodium channels. *Nature, Lond.* **242**, 459–461.

ARMSTRONG, C. M. & BEZANILLA, F. (1974). Charge movement associated with the opening and closing of the activation gates of the Na channels. *J. gen. Physiol.* **63**, 533–552.

CHANDLER, W. K., RAKOWSKI, R. F. & SCHNEIDER, M. F. (1976). Effects of glycerol treatment and maintained depolarization on charge movement in skeletal muscle. *J. Physiol.* **254**,285–316.

CHANDLER, W. K., SCHNEIDER, M. F., RAKOWSKI, R. F. & ADRIAN, R. H. (1975). Charge movements in skeletal muscle. *Phil. Trans. R. Soc.* B **270**, 501–505.

EBASHI, S., ENDO, M. & OHTSUKI, I. (1969). Control of muscle contraction. *Q. Rev. Biophys.* **2**, 351–384.

FALK, G. & FATT, P. (1964). Linear electrical properties of striated muscle fibres observed with intracellular electrodes. *Proc. R. Soc.* B **160**, 69–123.

GOLDMAN, D. E. (1943). Potential, impedance, and rectification in membranes. *J. gen. Physiol.* **27**, 37–60.

HARRIS, E. J. & BURN, G. P. (1949). The transfer of sodium and potassium ions between muscle and the surrounding medium. *Trans. Faraday Soc.* **45**, 508–528.

HODGKIN, A. L. & HOROWICZ, P. (1960). Potassium contractures in single muscle fibres. *J. Physiol.* **153**, 386–403.

HODGKIN, A. L. & HUXLEY, A. F. (1952). A quantitative description of membrane current and its application to conduction and excitation in nerve. *J. Physiol.* **117**, 500–544.

HODGKIN, A. L. & NAKAJIMA, S. (1972). Analysis of the membrane capacity in frog muscle. *J. Physiol.* **221**, 121–136.

HUXLEY, A. F. & STRAUB, R. W. (1958). Local activation and interfibrillar structures in striated muscle. *J. Physiol.* **143**, 40–41 *P*.

HUXLEY, A. F. & TAYLOR, R. E. (1958). Local activation of striated muscle fibres. *J. Physiol.* **144**, 426–441.

KEYNES, R. D. & ROJAS, E. (1973). Characteristics of the sodium gating current in the squid giant axon. *J. Physiol.* **233**, 28–30 *P*.

KEYNES, R. D. & ROJAS, E. (1974). Kinetics and steady-state properties of the charged system controlling sodium conductance in the squid giant axon. *J. Physiol.* **239**, 393–434.

MOBLEY, B. A., LEUNG, J. & EISENBERG, R. S. (1974). Longitudinal impedance of skinned frog muscle fibers. *J. gen. Physiol.* **63**, 625–637.

PEACHEY, L. D. (1965). The sarcoplasmic reticulum and transverse tubules of the frog's sartorius. *J. cell Biol.* **25**, 209–231.

PEACHEY, L. D. & SCHILD, RENE F. (1968). The distribution of the T-system along the sarcomeres of frog and toad sartorius muscles. *J. Physiol.* **194**, 249–258.

ROMANELLI, M. J. (1960). Runge–Kutta methods for the solution of ordinary differential equations. In *Mathematical Methods for Digital Computers*, vol. 1, ed. RALSTON, A. & WILF, H. S., pp. 110–120. New York: John Wiley and Sons.

SCHNEIDER, M. F. (1970). Linear electrical properties of the transverse tubules and surface membrane of skeletal muscle fibers. *J. gen. Physiol.* **56**, 640–671.

SCHNEIDER, M. F. & CHANDLER, W. K. (1973). Voltage dependent charge movement in skeletal muscle: a possible step in excitation-contraction coupling. *Nature, Lond.* **242**, 244–246.

SCHNEIDER, M. F. & CHANDLER, W. K. (1976). Effects of membrane potential on the capacitance of skeletal muscle fibers. *J. gen. Physiol.* (in the Press).

VALDIOSERA, R., CLAUSEN, C. & EISENBERG, R. S. (1974). Impedance of frog skeletal muscle fibers in various solutions. *J. gen. Physiol.* **63**, 460–491.

WARNER, ANNE E. (1972). Kinetic properties of the chloride conductance of frog muscle. *J. Physiol.* **227**, 291–312.